JOURNAL OF GEOPHYSICAL RESEARCH, VOL. 98, NO. D12, PAGES 23,501–23,523, DECEMBER 20, 1993

A Photostationary State Analysis of the NO_2-NO System Based on Airborne Observations From the Subtropical/Tropical North and South Atlantic

D.D. DAVIS,[1] G. CHEN,[1] W. CHAMEIDES,[1] J. BRADSHAW,[1] S. SANDHOLM,[1]
M. RODGERS,[1] J. SCHENDAL,[1] S. MADRONICH,[2] G. SACHSE,[3]
G. GREGORY,[3] B. ANDERSON,[3] J. BARRICK,[3] M. SHIPHAM,[3]
J. COLLINS,[4] L. WADE,[5] AND D. BLAKE[6]

The Chemical Instrumentation Test and Evaluation 3 (CITE 3) NO-NO_y database has provided a unique opportunity to examine important aspects of tropospheric photochemistry as related to the rapid cycling between NO and NO_2. Our results suggest that when quantitative testing of this photochemical system is based on airborne field data, extra precautions may need to be taken in the analysis. This was particularly true in the CITE 3 data analysis where different regional environments produced quite different results when evaluating the photochemical test ratio $(NO_2)_{Expt}/(NO_2)_{Calc}$, designated here as R_E/R_C. The quantity $(NO_2)_{Calc}$ was evaluated using the following photostationary state expression: $[NO_2]_{Calc} = (k_1[O_3] + k_4[HO_2] + k_5[CH_3O_2] + k_6[RO_2])[NO]_{Expt}/J_2$. The four most prominent regional environmental data sets identified in this analysis were those labeled here as free-tropospheric northern hemisphere (FTNH), free-tropospheric tropical northern hemisphere (FTTNH), free-tropospheric southern hemisphere (FTSH), and tropical-marine boundary layer (plume) (TMBL(P)). The respective R_E/R_C mean and median values for these four data subsets were 1.74, 1.69; 3.00, 2.79; 1.01, 0.97; and 0.99, 0.94. Of the four data subsets listed, the two that were statistically the most robust were FTNH and FTSH; for these the respective R_E/R_C mean and standard deviation of the mean values were 1.74 ± 0.07 and 1.01, ± 0.04. The FTSH observations were in good agreement with theory, whereas those from the FTNH data set were in significant disagreement. An examination of the critical photochemical parameters O_3, UV(zenith), NO, NO_2, and non-methane hydrocarbons (NMHCs) for these two databases indicated that the most likely source of the R_E/R_C bias in the FTNH results was the presence of a systematic error in the observational data rather than a shortcoming in our understanding of fundamental photochemical processes. Although neither a chemical nor meteorological analyses of these data identified this error with complete certainty, they did point to the three most likely possibilities: (1) an NO_2 interference from a yet unidentified NO_y species; (2) the presence of unmeasured hydrocarbons, the integrated reactivity of which would be equivalent to ~2.7 parts per billion by volume (ppbv) of toluene; or (3) some combination of points (1) and (2). Details concerning hypotheses (1) and (2) as well as possible ways to minimize these problems in future airborne missions are discussed.

INTRODUCTION

Since the early 1970s when photochemically generated free radicals became recognized as major atmospheric chemical drivers, there has been an increasing effort to quantify various aspects of what is now referred to as "fast photochemical theory." One of the more experimentally amenable components of this theory that lends itself to testing is the three-reaction sequence that couples NO to NO_2, i.e.,

(R1) $NO + O_3 \rightarrow NO_2 + O_2$

(R2) $NO_2 + h\nu \rightarrow NO + O$

(R3) $O + O_2 \xrightarrow{M} O_3$

From this reaction sequence it can be seen that atmospheric O_3 rapidly converts NO to NO_2 which during daylight hours is itself rapidly converted back to NO via reaction (R2). The time required for the cycling of NO to NO_2 and its return to the NO chemical form via (R1) and (R2) is typically of the order of a few minutes. Since this time is typically much shorter than either the production or the destruction of NO_x (NO + NO_2), it has been argued that through reactions (R1) and (R2) both NO and NO_2 should be in balance. In this case the relative atmospheric levels of these species can be defined by equation (1) [*Cadle and Johnson*, 1952; *Leighton*, 1961]:

$$\frac{[NO_2]}{[NO]} = \frac{k_1\,[O_3]}{J_2} \qquad (1)$$

Here the brackets denote the concentrations of a species and k and J denote the rate constants for the appropriate gas kinetic and photochemical process.

As related to the NO-NO_2 system, equation (1) is frequently given the label "simple photostationary state equation." We will also adopt this notation. An important aspect of this equation is the fact that it is defined in terms of measurable chemical species, and the rate parameters k_1 and J_2 also are reasonably well

[1]School of Earth and Atmospheric Sciences, Georgia Institute of Technology, Atlanta, Georgia.
[2]National Center for Atmospheric Research, Boulder, Colorado.
[3]NASA Langley Research Center, Hampton, Virginia.
[4]Science and Technology Corporation, Hampton, Virginia.
[5]Planning Research Corporation, Hampton, Virginia.
[6]University of California, Irvine, California.

Paper number 93JD02412.
0148-0227/93/93JD-02412$05.00

established. The recognized shortcoming of this equation is the fact that it does not consider other possible reaction channels in the conversion of NO to NO_2 [*Calvert and Stockwell*, 1983]. The most important of these involves the reactions of peroxy radicals, e.g.,

(R4) $HO_2 + NO \rightarrow NO_2 + OH$

(R5) $CH_3O_2 + NO \rightarrow NO_2 + CH_3O_2$

(R6) $RO_2 + NO \rightarrow NO_2 + RO$

(Note, RO_2 is used here to denote any organic peroxy radical other than CH_3O_2.) Reactions (R4) → (R6) lead to a modified expression for the NO-NO_2 photostationary state, e.g.,

$$\frac{[NO_2]}{[NO]} = \frac{(k_1[O_3]+k_4[HO_2]+k_5[CH_3O_2]+k_6[RO_2])}{J_2} \quad (2)$$

An important aspect of this expanded photostationary state equation is the fact that it shows NO being converted to NO_2 without the consumption of O_3. Under these conditions the chemistry defined by reactions (R4) → (R6) can act as a net source of O_3.

Although the addition of reactions (R4) → (R6) leads to an improvement in the overall chemical description of the NO-NO_2 system, an obvious shortcoming is the fact that any analysis using this equation requires reliable independent measurements of the transients HO_2, CH_3O_2, and RO_2. At this time, however, the instrumentation required for making reliable measurements of these species is still under development. Because of this experimental shortfall, most field sampling programs have focused on recording simultaneous measurements of the variables NO, NO_2, O_3 and the UV flux and/or $J(NO_2)$ via chemical actinometry; the free radical species HO_2, CH_3O_2, and RO_2 have been evaluated using photochemical models. The early urban studies of this type [*Stedman and Jackson*, 1975; *Calvert*, 1976; *Shetter et al.*, 1983] tended to show that the ratio of NO_2 to NO could be reasonably well represented by equation (1). For example, the dominant reaction involved in the conversion of NO to NO_2 was in these cases reaction (R1).

For rural or remote locations, where much lower NO_x levels lead to much higher total peroxy radical to O_3 ratios, experimental measurements of the NO_2/NO ratio were found to be in better agreement with equation (2) [*McFarland et al.*, 1978; *Ritter et al.*, 1979; *Fehsenfeld et al.*, 1983; *Parrish et al.*, 1986; *Trainer et al.*, 1987]. However, in nearly all of these cases, the major exception being the work reported by *Trainer et al.* [1987], to explain the observed NO_2/NO ratios required peroxy levels well in excess of model predictions.

Following several years of further development and testing of NO, NO_x and NO_2 measurement techniques [*Hoell et al.*, 1987; *Gregory et al.*, 1990*a*, *b*], more recent NO-NO_2-O_3 photostationary state studies appear to be giving more encouraging results [*Chameides et al.*, 1990; *Ridley et al.*, 1992]. In National Aeronautics and Space Administration's (NASA's) Chemical Instrumentation Test Evaluation 2 (CITE 2) airborne field program, two independent NO-NO_2 data sets were generated using instrumentation which involved two different measurement techniques [*Chameides et al.*, 1990]. The focus of the latter study was on relatively clean tropospheric air. The analysis, as presented by *Chameides et al.*[1990], indicated that "simple photostationary theory" predicted NO_2/NO ratios that were a factor of 1.6 to 2.0 lower than the observations. By contrast, equation (2) resulted in an average calculated NO_2/NO ratio that was only a factor of 1.25 lower than the observed ratio.

The (Mauna Loa Observatory Photochemical Experiment) (MLOPEX) on the island of Hawaii represents perhaps one of the most comprehensive photochemical studies carried out in recent years [*Ridley and Robinson*, 1992; *Ridley et al.*, 1992]. During a 1-month field study in the spring of 1988, several thousand NO and NO_2 observations were recorded under clear sky conditions. The latter data together with ancillary measurements permitted an in-depth examination of photochemical theory under well-defined atmospheric conditions of solar flux and chemical composition. The results from this study were examined in terms of the photochemical expression:

$$\phi = \frac{J_2[NO_2]}{k_1[NO][O_3]} \quad (3)$$

Based on the MLOPEX observations, values of Φ were typically higher than unity, approaching 2.0 for high Sun conditions. The difference between the predicted value of Φ based on simple photochemical theory (i.e., 1.0) and that estimated from field observations was then used to estimate the total peroxy radical mixing ratio. As related to the testing of the NO_2-NO photostationary state, the MYLOPEX results, based on reactions (1)-(6), showed excellent agreement with the experimental observations (e.g., within ± 10%).

Although collectively the above results can be viewed as quite encouraging, both from an experimental and from a theoretical perspective, we believe potentially important unresolved issues may still remain. This is particularly true in the case of the aforementioned CITE 2 airborne data sets where the reported average value for the observed NO_2/NO ratio was given as approximately 1.25 times larger than the value estimated from equation (2). This difference, although modest in magnitude, is nevertheless well outside of the quoted standard deviation of the mean, e.g., ± 5%. Furthermore, because *Chameides et al.* [1990] based their analysis on what was defined as a "calculated ratio difference" approach, the analysis tended to underweight high values of the ratio $(NO_2/NO)_{Expt}$. Following an analysis approach similar to that taken in this paper, these authors have found that the level of disagreement between $(NO_2/NO)_{Expt}$ and $(NO_2/NO)_{Calc}$ was approximately a factor of 1.5, the experimentally measured ratio being higher. Possible reasons for this level of disagreement include that (1) theory, as defined by equation (2), is chemically incomplete; (2) the peroxy radical concentrations calculated from the model are in error due to

systematic errors in the J and k values employed, or (3) that there are undefined sources of systematic error in the input observational data.

Concerning the latter possibility, it is important to recognize that because of the limited number of individual sample runs recorded during an airborne field experiment, the typical data analysis approach has involved an evaluation of an "ensemble" mean value for the NO_2/NO ratio. The potential difficulty with this approach is that in airborne field sampling it is quite common to encounter a wide range of air mass types over a relatively short time period. Thus a systematic error in any one of the critical photochemical parameters in any one of these different environment regimes can potentially lead to a systematic shift in either the experimental or the calculated ratio of NO_2/NO. In principle, if all chemical species required for interpreting the NO_2-NO chemistry were measured and measured correctly and all processes influencing the NO_2/NO ratio were accounted for in the form of some version of equation (2), the need for segregating data according to the type of environment sampled would be small. In actual fact, the first condition is almost never strictly satisfied either for airborne or for ground-based studies. But in the case of airborne studies, this problem has the potential for becoming acute.

The purpose of this work will be to further explore how well we understand the NO-NO_2-O_3 photostationary state system in the context of some of the questions raised in the above text. In carrying out this analysis, we will be examining an NO-NO_2 database recently recorded during the second phase of the NASA GTE/CITE 3 airborne field mission. The sampling region encompassed by these data included the subtropical/tropical North and South Atlantic Ocean, as shown in Figure 1.

MODEL DESCRIPTION

The photochemical box model used in the evaluation of the CITE 3 database was similar to that previously described by *Chameides et al.* [1987, 1989]. The current model contains 60 H_xO_y-N_xO_y-CH_4 gas kinetic reactions, 130 hydrocarbon reactions, 8

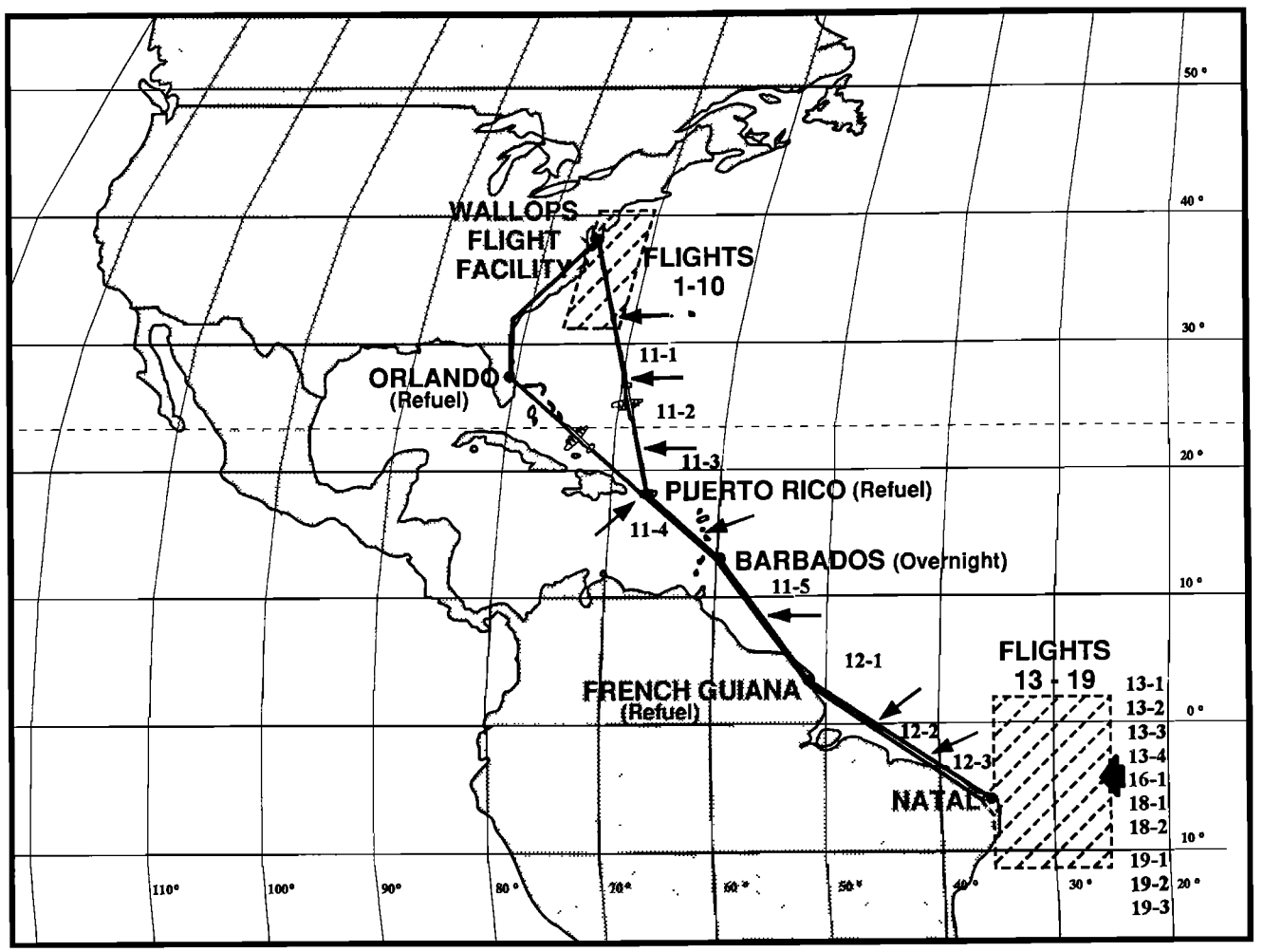

Figure 1. Chemical Instrumentation Test and Evaluation (CITE) 3 flight track. NO-NO_2 data sampling periods are indicated along flight track with flight number designations 11-1, 11-2, 11-3, 11-4, 11-5, 12-1, 12-2, 12-3, 13-1, 13-2, 13-3, 13-4, 16-1, 18-1, 18-2, 19-1, 19-2, and 19-3.

heterogeneous removal steps, and 13 photolytic reactions. The N_xO_y-O_3-CH_4 rate coefficients were taken from the NASA JPL publication 92-20 [*Demore et al.*, 1992]. The heterogeneous rate coefficients were based on those recommended by *Logan et al.* [1981], and the photolytic J values were calculated using a two-stream radiative transfer model, as discussed below.

The chemical oxidation of non-methane hydrocarbons (used to evaluate the quantity RO_2) was based on the reaction scheme and rate coefficients given by *Lurmann et al.* [1986]. In our model we used the "condensed hydrocarbon" oxidation mechanism; however, this scheme was modified to include organic peroxide/OH reactions. In addition, several of the stoichiometric NO reactions were replaced by actual elementary processes, as discussed by *Jacob and Wolfsy et al.* [1988]. The latter adjustment was designed to reflect the low NO_x environment encountered in the tropical Atlantic Ocean.

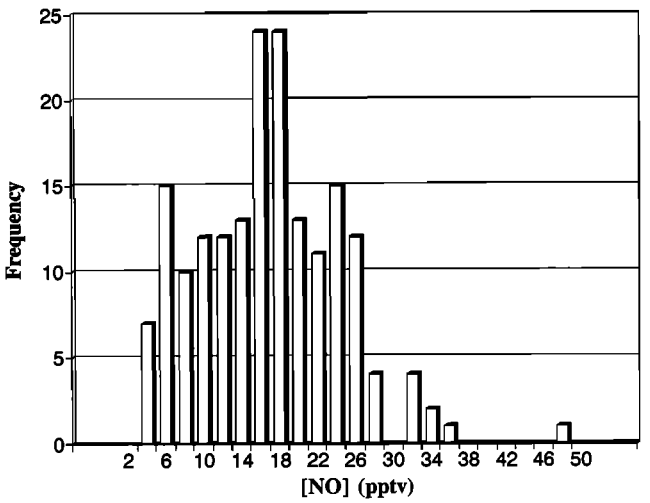

Figure 2*a*. Concentration frequency distributions for NO based on signal-to-noise (S/N) data filtering at the >2:1 level. All "plume" data have been removed.

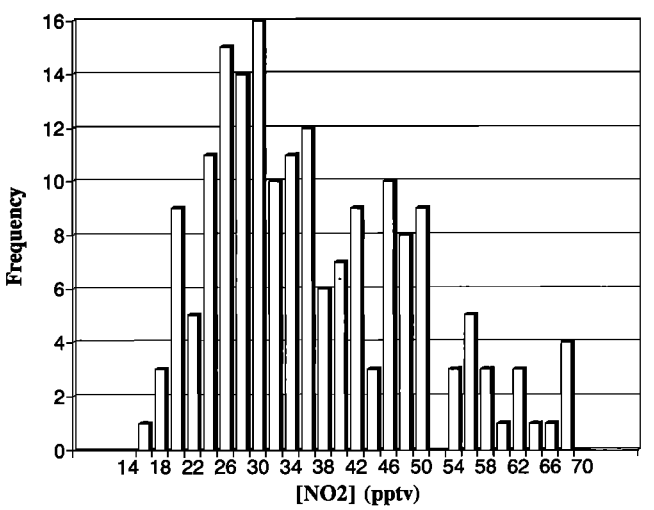

Figure 2*b*. Concentration frequency distributions for NO_2 based on S/N data filtering at the >2:1 level. All "plume" data have been removed.

The basic input to our model consisted of fixed values for the mixing ratios of the chemical observables O_3, NO, H_2O, CO and the physical parameters, temperature, pressure, and UV flux. In the case of H_2 and CH_4 we assumed globally average values for the mixing ratios, e.g., 0.55 and 1.7 parts per million by volume (ppmv), respectively. The concentrations of the short-lived species HO_2, OH, $O(^1D)$, CH_3O, CH_3O_2, RO_2, NO_2, and NO_3 as well as the chemically related species CH_2O, HO_2NO_2 and N_2O_5 were calculated by setting the rate of production for each species equal to the rate of destruction, i.e., the condition of photochemical equilibrium. For most runs the intermediate-lived species such as HNO_3, H_2O_2, and CH_3OOH were also assumed to have concentrations typical of photochemical equilibrium conditions. However, to assess the possible magnitude of error resulting from the latter assumption, the concentration levels of the intermediate-lived species were also evaluated for a limited number of runs using a time-dependent box model. In the latter case, the observed values for CO, H_2O, O_3, T, and P for a given run at a specified altitude and geographical coordinates were assumed to be representative of the daily average values for these parameters. To establish the diurnal concentration profile for NO, a flux was assigned to NO such that the model-estimated NO concentration agreed with the observed value for the observation time of day. The results from these time-dependent model evaluations gave OH values that ranged from 10% higher to 10% lower than the photostationary state calculations, the average being +1% higher. Thus the net effect on the value of $(NO_2/NO)_{Calc}$ was found to be negligibly small.

A comparison of our calculated OH values (for marine boundary layer conditions) with model-calculated values of Saltzman (private communication, 1993) and M. Thompson (private communication, 1993) showed the latter modelling results to be within -20% and +5%, respectively.

Photolytic rate constants were evaluated for each observational time period using the results from a two-stream radiative transfer model [*Dickerson et al.*, 1979]. The solar flux used in these calculations was for cloud-free conditions. Our J value estimates were based on a surface albedo of 7%. The principal factor used to adjust the model calculated J values to actual conditions in the field (e.g., clouds, haze, and aerosol scattering) was an empirically derived cloud correction factor (CCF). This scaling factor was assumed to be wavelength independent and was defined in terms of the ratio $J(NO_2)_{Expt}/J(NO_2)_{TS}$, where $J(NO_2)_{TS}$ is the calculated J value for NO_2 from the two-stream model. The quantity $J(NO_2)_{Expt}$ was evaluated using the airborne observational UV flux data as determined from real-time upward and downward looking UV Eppley photometer readings. The latter readings were used in conjunction with a modified semiempirical formula [*Chameides et al.*, 1990; *Madronich*, 1987], e.g.,

$$J(NO_2)_{Expt} = \frac{1.35E_u}{(0.56+0.03z)\cos\theta+(0.21-0.015z)} + 2(1.14)E_d \quad (4)$$

TABLE 1*a*. CITE 3 NO, NO_2, and Ancillary Measurements

MISSION	Time GMT Start	Time GMT Stop	Alt Avg, km	Lat Avg, deg	Long Avg, deg	UV, MW/cm^2 U Zenith	UV, MW/cm^2 U Nadir	Temp Avg °K	Dew Point, °C Avg	Dew Point, °C Range, Max/Min
11-1	1330	1455	3.9	32.1	72.8	3.6	0.8	277	-29	-8/-38
11-2	1508	1555	4.5	26.2	70.6	5.0	1.0	275	-19	-12/-32
11-3	1605	1706	5.1	21.5	68.6	5.5	1.1	272	-27	-20/-37
11-4	1718	1734	0.2	18.8	66.3	4.4	0.3	300	23	24/23
11-5	1958	2033	4.6	15.5	62.0	2.3	0.6	274	-14	-12/-24
12-1	1256	1351	3.9	8.5	55.5	4.8	0.7	277	2	2/1
12-2	1718	1744	3.9	-0.8	49.0	4.6	1.6	276	-27	-17/-33
12-3	1806	1939	4.5	-2.6	43.7	2.5	0.5	273	-32	-29/-35
13-1	1456	1540	2.0	-8.6	33.1	5.2	0.6	286	0	7/-8
13-2	1558	1653	5.1	-9.4	33.4	4.9	0.9	271	-38	-33/-42
13-3	1702	1708	1.8	-6.9	33.1	3.4	0.5	287	3	4/2
13-4	1718	1724	0.2	-6.7	33.6	2.8	0.2	298	20	20/20
16-1	1540	1634	0.3	-3.1	29.4	3.4	0.3	297	21	21/21
18-1	0938	1009	2.7	-5.5	31.3	2.1	0.5	284	-21	-19/-23
18-2	1018	1044	4.5	-5.4	31.6	3.0	0.8	273	-31	29/-32
19-1	1727	1755	1.5	-5.5	31.3	2.2	0.4	291	-2	-1/-4
19-2	1808	1836	2.7	-5.5	31.1	1.5	0.5	285	-19	-7/-23
19-3	1849	1858	5.1	-5.4	31.7	1.1	0.4	270	-33	-32/-33

MISSION	O_3, ppbv Avg	O_3, ppbv Range, Max/Min	CO, ppbv Avg	CO, ppbv Range, Max/Min	NO, pptv Avg	NO, pptv Range, Max/Min	NO_2, pptv Avg	NO_2, pptv Range, Max/Min	NO_y, ppbv Avg	NO_y, ppbv Range, Max/Min
11-1	52	63/43	92	115/81	19	25/10	47	69/18	1.7	3.2/0.9
11-2	49	56/44	95	110/85	16	32/7	36	54/18	3.7	6.3/1.3
11-3	60	88/48	69	85/62	23	47/14	28	48/18	2.7	3.9/1.4
11-4	48	80/29	169	275/94	50	84/23	216	367/87	8.3	9.7/6.1
11-5	42	55/35	78	83/72	11	23/7	29	35/19	2.2	2.7/1.6
12-1	24	25/21	82	85/76	6	11/2	26	49/15	3.1	3.3/3.0
12-2	66	72/54	83	89/79	19	24/16	26	34/16	0.9	1.3/0.7
12-3	82	89/77	96	107/83	21	28/14	40	65/17	1.4	2.1/1.0
13-1	54	61/48	100	110/96	6	11/3	25	32/14	1.3	1.6/0.7
13-2	70	75/63	87	93/84	28	37/20	33	48/21	0.5	0.7/0.4
13-3	55	58/53	114	116/112	6	8/4	25	31/20	2.8	2.9/2.8
13-4	39	42/35	93	94/93	139	202/61	316	455/207	3.3	3.5/2.8
16-1	33	34/31	136	141/132	5	7/3	22	36/15	5.5	5.7/5.3
18-1	83	88/71	88	93/85	14	17/11	46	62/35	1.1	1.3/1.0
18-2	80	82/78	97	98/95	23	26/20	31	46/17	1.2	1.2/1.0
19-1	69	71/64	137	143/125	14	19/10	36	46/17	2.0	2.4/1.7
19-2	76	83/70	104	109/94	16	19/13	45	61/30	1.2	2.2/0.9
19-3	71	73/68	91	92/88	17	22/15	28	33/24	1.2	1.3/1.2

where z is the altitude (in kilometers), θ is the solar zenith angle, and E_u and E_d are the upward and downward looking Eppley readings (watts per square centimeter).

As noted above, the ratio of $J(NO_2)_{Expt}/J(NO_2)_{TS}$ was used to scale all other J_{TS} values without additional wavelength correction. Although obviously an oversimplification, at present this appears to be the only direct way for adjusting other J values for actual cloud/haze conditions. For the CITE 3 NO-NO_2 data set analyzed here, the ratio, $J(NO_2)_{Expt}/J(NO_2)_{TS}$, ranged from a low value of 0.8 to a maximum of 1.3 and had an average value of 1.08. In nearly all cases the low values were correlated with overhead clouds, whereas ratios > 1.0 appeared to be generally correlated with observable clouds below the aircraft. Based on the recent work of *Shetter et al.* [1992] in which Eppley-derived $J(NO_2)$ values were compared directly with NO_2 chemical actinometry, we estimate the overall 2σ uncertainty in our $J(NO_2)$ values to be ± 15%. The latter uncertainty thus reflects the uncertainty in the application of equation (4) and the uncertainty in the measured airborne UV flux. The potential systematic error in the two-stream model calculated $J(NO_2)$ and other J values is more difficult to assess; however, based on estimated uncertainties in absorption cross sections and uncertainties arising from the application of specific radiative transfer models, we estimate the magnitude of this error could be as large as 20%.

TABLE *1b*. CITE 3 Hydrocarbon Measurements

Mission	Time, (UT)	Alt., km	C_2H_6, ppbv	C_2H_4, ppbv	C_2H_2, ppbv	C_3H_8, ppbv	C_3H_6, ppbv	C_4H_{10}, ppbv	OH-Equiv. C_3H_8, ppbv	NMHC Level
11-1	1307	3.27	0.71	0.04	0.04	0.14	0.03	LOD	1.44	1
11-1	1416	3.91	0.57	0.01	0.05	0.06	0.01	LOD	0.76	1
11-2	1513	4.53	0.69	0.03	0.08	0.09	0.02	LOD	0.83	1
11-3	1610	5.14	0.52	0.04	0.02	0.07	0.03	LOD	1.44	1
11-4	1707	5.14	0.85	0.02	0.05	0.17	0.03	LOD	1.34	1
12-1	1257	3.92	0.40	0.09	0.07	0.05	0.08	LOD	3.30	1
12	1359	3.28	0.34	0.03	0.03	0.02	0.02	LOD	1.09	1
12-2	1721	3.91	0.42	0.03	0.02	0.01	0.12	LOD	3.88	1
13	1313	3.33	0.85	0.15	0.36	0.27	LOD	0.24	2.63	1
13-1	1510	1.96	0.41	0.04	0.07	0.04	0.03	LOD	1.35	1
13-2	1624	5.13	0.91	0.52	0.29	0.25	LOD	0.28	6.39	2
14	1511	1.48	1.00	0.81	0.52	0.60	0.02	0.33	10.24	3
14	1707	1.50	1.29	0.57	0.54	0.43	0.05	0.46	9.15	2
16	1508	1.49	1.06	0.89	0.69	0.82	0.25	0.48	18.65	3
16-1	1555	0.28	0.84	0.32	0.36	0.41	0.11	0.26	7.88	2
16	1730	1.49	1.16	1.07	1.03	0.53	0.32	0.63	22.66	3
18	0919	1.48	1.04	0.70	0.59	0.34	0.05	0.42	10.02	3
18-1	0956	2.70	1.44	0.43	0.88	1.06	0.12	0.53	10.62	3
18-2	1037	4.52	0.83	0.44	0.30	0.25	LOD	0.25	5.41	2
19-1	1744	1.44	1.13	1.27	0.64	0.24	0.07	0.52	16.32	3
19-2	1825	2.69	1.49	1.79	0.65	0.27	0.17	0.53	24.54	3

Level 1, equivalent C_3H_8 range (0-5 ppbv), model value 2.5 ppbv. Level 2, equivalent C_3H_8 range (5-10 ppbv), model value 7.5 ppbv. Level 3, equivalent C_3H_8 range (10-25 ppbv), model value 25 ppbv. LOD, limit of detection, typically < 0.02 ppbv.

OBSERVATIONAL DATABASE

The species NO, NO_2, and NO_y (where $NO_y = NO + NO_2 + NO_3 + N_2O_5 + HNO_3 + HO_2NO_2 + PAN + RNO_x$) were measured simultaneously using the two-photon/laser-induced fluorescence (TP/LIF) technique [*Bradshaw et al.*, 1985; *Sandholm et al.*, 1990, 1992]. This spectroscopically selective NO technique simultaneously determined ambient NO, NO produced from the photolysis of ambient NO_2, and NO produced from the reduction of ambient NO_y compounds. The latter process involved the use of a 300°C gold catalytic surface with 0.3% CO as a reducing agent. The photolytic conversion of NO_2 to NO was achieved using a 1-kW filtered UV-arc continuum-light source having a passband of 350 nm $<\lambda<$ 410 nm. The photolytic yield ranged from 30% to 60% and sample residence times ranged from 2 to 4.5 s. A porcelain-glass- coated common inlet was used to sample ambient air in an orientation perpendicular to the airstream. Constant volumetric flow (circa 250 lpm) and, consequently, sample residence time (circa 0.25) was maintained throughout this common sampling inlet manifold. Three separate LIF sampling cells were used: one each for measuring the LIF signal from ambient NO, photolytically produced NO from NO_2, and catalytically produced NO from NO_y. Flow from the common inlet manifold was split at a position near (e.g., <0.5 m) each detection system.

Standard addition calibrations using NO and NO_2 were routinely carried out by injecting a known concentration of standards into the common ambient sampling manifold. All flows were measured using linear mass flow meters that had been cross compared to volume displacement standards. The accuracy of these instrument calibrations has been estimated at ± 16% for NO and ± 18% for NO_2 and NO_y at the 95% confidence limit. Limits of detection for a typical 3-min signal integration period were 2.5 parts per trillion by volume(pptv) for NO and 12 pptv for NO_2, based on a signal-to-noise ratio of 2:1. The typical ± 10% at 500 pptv, increasing to ± 20% at 200 pptv.

The NO-NO_2 database used in this study was recorded during the Brazilian/tropical South Atlantic component of the CITE 3 program plus the transit flights from Wallops Island, Virginia, to Natal, Brazil. These data were recorded during missions 11A, 11B, 12A, 12B, 13, 16, 18, and 19, covering the time period September 9-September 30, 1989 (i.e., see Figure 1). Missions 11A, 11B, 12A, and 12B define the transit flight from Wallops Island, Virginia to Natal, Brazil, and were all over water or the Brazilian coastline. No data from missions 15 and 17 were used since they were both nighttime missions. In addition, no data were used for flight 14 (a daytime flight) since one of the critical parameters required for our analysis, NO_2, was not measured on this mission. For details on the geographical coverage of each mission, see Hoell et al., this issue.

The north/south tropical Atlantic CITE 3 database, as defined by missions 11-19, consisted of 231 independent NO-NO_2 measurements. Of the 231 total data points, 190 of these had (S/N) signal/noise ratios of >2:1, and 120 had signal/noise (S/N) values ≥3:1. The S/N designation as used in this text will always mean that both NO and NO_2 satisfy the indicated signal-to-noise ratio criteria. As will be discussed in greater detail below, our purpose in S/N filtering the NO-NO_2 database was to assess

the possible influence of systematic errors (specifically offset errors) and to assess the statistical robustness of several data subsets of the total database. The authors note that in the case of offset errors, any attempt to salvage low S/N data by assigning weighting factors to them can be dangerous since, on average, low S/N data (reflecting low mixing ratios) are more prone to being influenced by offset errors than high S/N data. The assignment of a weighting factor to individual data points implies that in all cases the major error associated with the data is random in nature. Quite clearly, this is not always the case.

Figures 2*a* and 2*b* show concentration/frequency distribution plots for NO and NO_2 for those data having a S/N ratio of > 2:1. The only data pairs excluded from Figures 2*a* and 2*b* are those we have labeled later in the text as "plume" data. The latter data were primarily recorded in the marine boundary layer in the near vicinity of the island of Puerto Rico and clearly show evidence of an island anthropogenic effect. This small data set (e.g., 10 NO-NO_2 data pairs) is unique in that it represents the only NO-NO_2 data recorded during the CITE 3 tropical Atlantic campaign in which moderate levels of NO and NO_2 were observed. "Moderate," in this case, means NO_2 mixing ratios of 90 to 450 pptv and NO of 20 to 150 pptv. In continental United States, these levels would most likely be classified as relatively clean rural air. In the tropical Atlantic, typical boundary layer mixing ratios for NO_2 and NO were 21 and 5 pptv, respectively. Thus for purposes of discussion in this text we have used the labelling "tropical-marine boundary layer (plume)" to describe these data.

Figures 2*a* and 2*b* indicate that based on a S/N filter level of > 2:1, NO and NO_2 mixing ratios ranged from 4 to 48 pptv and 16 to 69 pptv, respectively. The median values for NO and NO_2 were 17 and 35 pptv, respectively. When filtered at the 3:1 S/N level, the range in NO and NO_2 decreased to 6 to 32 pptv and 24 to 69 pptv, respectively. For the latter case, the median value for NO was 17 pptv and that for NO_2 was 40 pptv, indicating that NO_2 had a greater sensitivity to S/N filtering than did NO.

Tables I*a* and I*b* provide the average and maximum/minimum values recorded for NO and NO_2 during each NO-NO_2 sampling period as well as the corresponding average and maximum/minimum values for the most relevant ancillary measurements. The latter included CO, dew point, NO_y, O_3, temperature, pressure, UV (zenith), UV (nadir), and non-methane hydrocarbons. For this data set, a "sampling period" has been defined as a time period during which there were at least two sequential independent measurements of NO and NO_2 under near-constant altitude conditions. The general location of each of these sampling periods is shown in Figure 1.

Table 1b summarizes the results from the analysis of select C_2-C_4 hydrocarbon grab samples. Only those samples collected geographically, altitudinally, and temporally close to NO-NO_2 sampling time periods have been reported. They represent 82% of the total of 28 grab samples taken during the CITE 3 (Brazilian) campaign. These samples were collected using precleaned evacuated stainless steel 2- or 6-Liter cans which were typically pressurized to 2 atm. The analysis of these samples was carried out after the completion of the CITE 3 field campaign using gas chromatographic procedures as discussed by Martinez [1991] and Blake et al. [1992]. Further details on other ancillary measurements recorded during CITE 3 can be found in the paper by *Hoell et al.* [this issue].

DATA ANALYSIS

Figure 3 shows a frequency distribution plot that graphically summarizes the results from our analysis of the CITE-3 NO-NO_2 database. In this plot the X axis is defined in terms of the dimensionless quantity R_E/R_C where $R_E=(NO_2/NO)_{Expt}$ and $R_C=(NO_2/NO)_{Calc}$. However, the latter ratio is more accurately represented by the quantity $(NO_2)_{Calc}/(NO)_{Expt}$ since $(NO)_{Expt}$ is used in the modelling calculations. In this case the ratio R_E/R_C reduces to $(NO_2)_{Expt}/(NO_2)_{Calc}$. Given then that the following criteria are met: (1) that all critical variables have been measured, (2) that the measurements are free of major errors, (3) that the chemistry of the NO-NO_2 system is correctly represented by equation (2), and (4) that the model has accurately estimated the concentrations of the critical radical species HO_2, CH_3O_2, and RO_2; the significance of the ratio R_E/R_C is that the median value for R_E/R_C for a specified data set should be unity (see below for a more detailed discussion of this topic). Significant departure from unity thus signifies a potential problem in any one or all of the above areas.

The data presented in Figure 3 are for an S/N filter level of > 2:1. Only NO-NO_2 data at the > 2:1 S/N level have been used since only these data were deemed acceptable for a preliminary quantitative assessment of equation (2). Recall that the LIF limit-of-detection for NO and NO_2 was defined in terms of S/N = 2:1.

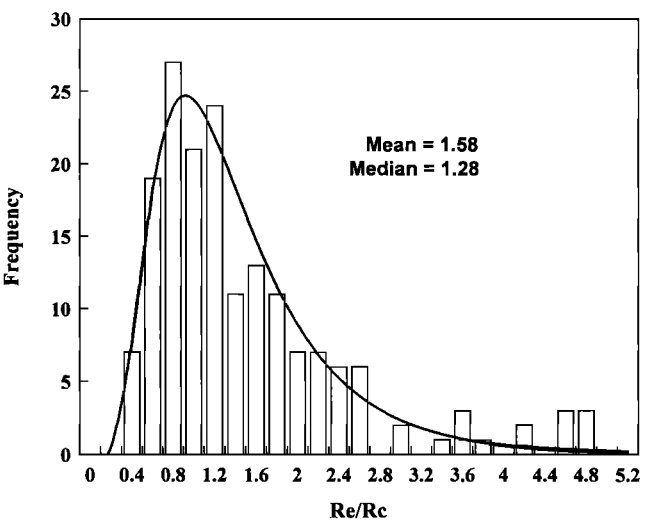

Figure 3. R_E/R_C frequency distribution plot based on S/N data filtering at the >2:1 level. The continuous lognormal curve was generated using the log-transformed mean and standard deviation of the data set. All "plume" data have been removed.

The data plotted in Figure 3 reveal several interesting features. For example, when referenced to the continuous lognormal curve shown in the figure, the distribution is seen to have the general characteristics of a lognormal distribution. The fact that this type of distribution is found is not totally surprising since all values of R_E/R_C are necessarily confined to positive numbers, and the expected median value is unity. Statistically, a common distribution that arises from these restrictions is one that is lognormal. The continuous lognormal curve shown in Figure 3 was derived from the statistical characteristics of the log-transform distribution, e.g., the mean and the standard deviation.

Still another interesting qualitative feature of the R_E/R_C frequency distribution plot is the apparent multimode structure of this distribution. In this case there appears to be at least two separate modes and quite possibly three.

From a quantitative point of view the frequency versus R_E/R_C plot also raises an interesting question as related to the comparison of model predictions with theory. For example, the mean R_E/R_C values for data filtered at S/N > 2:1 and ≥ 3:1 were 1.58 and 1.53, respectively; and the median values were 1.29 and 1.34, respectively. It may be recalled that the mean R_E/R_C value for the re-analyzed CITE 2 airborne data set [*Chameides et al.*, 1990] was also approximately 1.5, and the corresponding median value has been estimated at 1.33. Thus at the "ensemble" data analysis level, the CITE 2 and CITE 3 data sets give quite similar results. For both data sets the "expected" median value for the ratio R_E/R_C (e.g., for the case of perfect conditions experimentally and theoretically) would be unity. This follows from the fact that under perfect conditions the median values for R_E and R_C would be equal. Therefore it is the median that defines a "reference point" for comparison of observations with theory [*Hines and Montgomery*, 1972]. Under these same perfect conditions the "expected mean", EM, for R_E/R_C would be given by:

$$\left(\frac{R_E}{R_C}\right)_{EM} = \exp\left(\frac{S^2}{2}\right) \quad (5)$$

where S^2 is the variance, as defined by the log-transform plot of R_E/R_C [*Hines and Montgomery*, 1972].

In the case of the CITE 3 database the median value of R_E/R_C is seen to be significantly shifted relative to the expected value of 1.0, thus suggesting the presence of one or more problems in our understanding of the relevant photochemical processes related to the NO-NO_2 system and/or in the quality of the input data to the model. In this context, it is quite significant that the CITE 3 database shows strong evidence of being composed of two or more independent distributions.

The latter conclusion is further supported by the results from a scatter plot of the quantities $(NO_2)_{Expt}$ and $(NO_2)_{Calc}$, as shown in Figure 4. In this plot we have attempted to optimize any inherent correlation between these two quantities by using only data filtered at the S/N ≥3:1 level. In addition, all high mixing ratio NO-NO_2 plume data identified earlier in the text (10 points) were removed. Because of the noisy nature of these data, we also have displayed them in the form of a "bin" plot as shown in Figure 5. In this case the X axis was divided into ten concentration bins where each bin was assigned 11 data points. The results from the latter plot make more apparent that there is a positive correlation between $(NO_2)_{Calc}$ and $(NO_2)_{Expt}$; but the magnitude of this correlation is very modest, resulting in a Pearson r^2 value of only 0.30.

The authors note that a strong correlation between $(NO_2)_{Calc}$ and $(NO_2)_{Expt}$ does not in itself provide a quantitative assessment of the agreement between theory and observation since $(NO_2)_{Calc}$ is itself evaluated using $(NO)_{Expt}$. However, a strong correlation does suggest that most of the data being examined have similar photochemical characteristics, even though the weighting factor for each of these characteristics in $(NO_2)_{Expt}$ versus $(NO_2)_{Calc}$

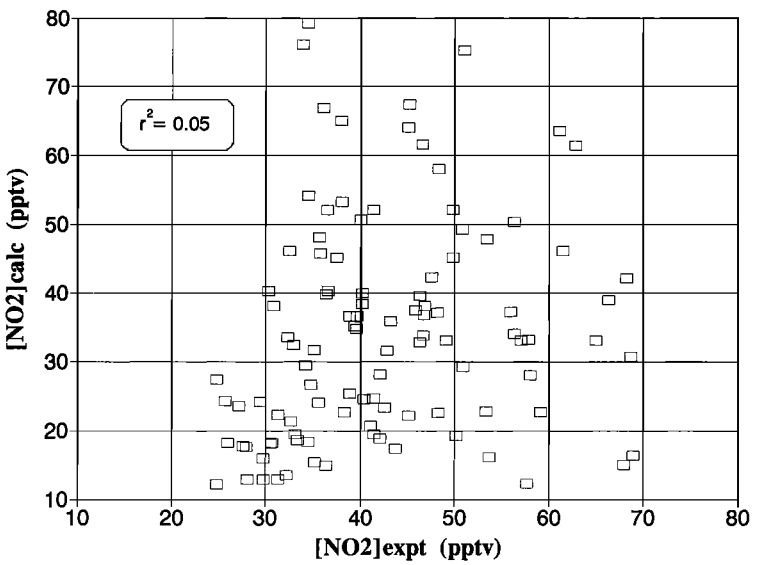

Figure 4. Scatter plot of experimentally observed NO_2 mixing ratios versus model-calculated NO_2 mixing ratios. Data set consists of all data pairs having S/N ≥3:1. All "plume" data have been removed.

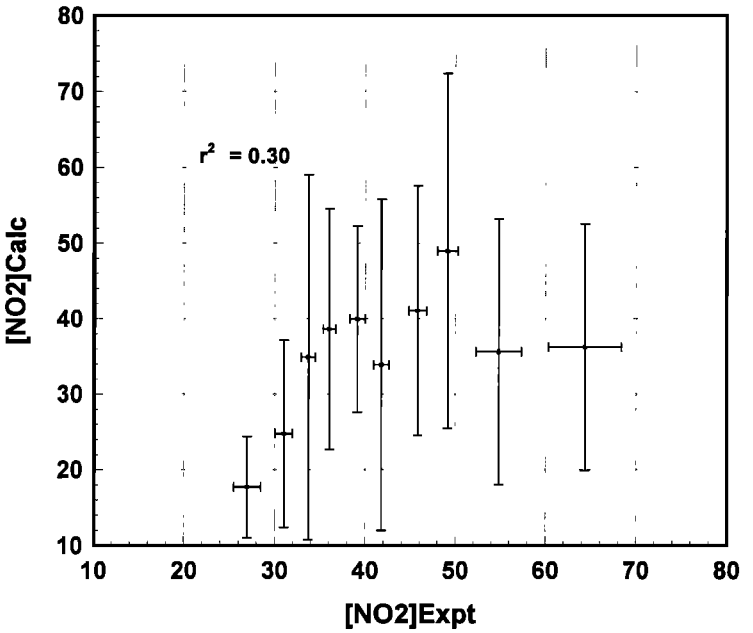

Figure 5. Regression plot of experimentally observed NO_2 mixing ratio versus model-calculated NO_2 mixing ratio. Data consist of all data pairs having S/N ≥3:1. All "plume" data have been removed. Data points have been divided into 10 bins having an equal number of data points per bin. Horizontal and vertical bars represent the standard deviation of the "binned" observational and calculated values of NO_2.

might be systematically different. A weak correlation, on the other hand, could mean that large random errors exist in the key variables $(NO_2)_{Expt}$ and $(NO)_{Calc}$, that the range of values for the key variables was too limited, or that the overall data set was made up of two or more distributions having different chemical properties which were not accurately reflected in the model calculations. Our assessment of the weak correlation coefficient derived from this analysis is that the latter possibility is the most likely one. For all of the above reasons, we have concluded that further analysis of the full data set would be relatively unproductive. In the text that follows, therefore, our analysis of the CITE 3 NO-NO_2 data is focused on (1), regrouping the full data set into statistically robust subsets and, (2), the quantitative photochemical analysis of these subsets in terms of both random and potential systematic errors.

To help identify potentially robust data subsets contained within the full database, we have examined the latter in terms of two geophysical parameters: latitude and altitude. Both parameters tend to subdivide the atmosphere into regions having major chemical gradients and thus potentially define appropriate environmental regimes for more detailed analysis. Figures 6*a*-6*b* and 7*a*-7*d* illustrate this approach. In these figures all calculated R_E/R_C values as well as the values of several ancillary measurements (i.e., NO_x, NO_y, CO, and O_3) have been independently plotted as a function of latitude and altitude. The latter plots were generated based only on those sampling runs where the NO-NO_2 data had an S/N value of >2:1. For the latitudinal profiles the R_E/R_C values and mixing ratios for each chemical variable were binned every 5° of latitude and all data were for altitudes ≥2.5 km. The error bars shown in these figures represent the standard deviation calculated from all data averaged in each 5° bin.

The results from these plots indicate the following: (1) the latitudinal R_E/R_C data show a very clear systematic difference between the northern and the southern hemisphere, with the northern hemispheric values being significantly higher than those in the southern hemisphere. Within the northern hemisphere there also appears to be two independent data groupings. (2) Based on a visual inspection, the latitudinal trends in R_E/R_C appear to be positively correlated with NO_y but are anticorrelated with the general trend in O_3. Both CO and NO_x show no simple correlation with the R_E/R_C trends. (3) The altitudinal trends in the southern hemisphere appear to be a strong function of the S/N filter level. For example, the ≥3:1 filtered data show R_E/R_C values centered around 1.0 for high altitudes (z ≥ 3.7 km), dropping to a little less than 1 for middle altitudes (2.2 - 3 km) and then dropping to considerably less than 1 (e.g., 0.60) for altitudes corresponding to the trade wind inversion (1.3 - 2.2 km). By contrast, databased on a S/N range of 2:1 to 3:1 show R_E/R_C values centered around 1.0 for very low altitudes (boundary layer); but for the trade wind region, most R_E/R_C values are far greater than unity. The R_E/R_C distribution at still higher altitudes is similar to that for the 3:1 S/N filtered data set. The critical variables CO and NO_y show no simple trends relative to R_E/R_C and altitude. (The authors note that only in the southern hemisphere was there sufficient data as a function of altitude to look for possible trends.)

Based on the trends in R_E/R_C as well as the general trends in the ancillary measurements (Figures 6*a*-6*b*, 7*a*-7*d*), we have concluded that the bulk of the CITE 3 NO-NO_2 data can be assigned to three major data subsets. These have been labeled here as free-tropospheric northern hemisphere (FTNH), free-tropospheric tropical northern hemisphere (FTTNH), and free-tropospheric southern hemisphere (FTSH). These three regional

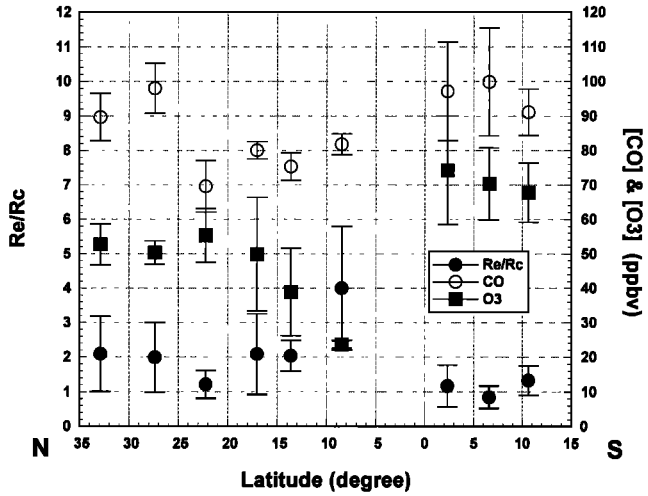

Figure 6*a*. Latitudinal variation in the mean values of R_E/R_C, CO, and O_3. Data have been "binned" into 5° latitudinal increments. Error bars for each mean value reflect the standard deviation for the data within the bin. The altitude in all cases is >2.5 km. All data pairs have S/N values >2:1.

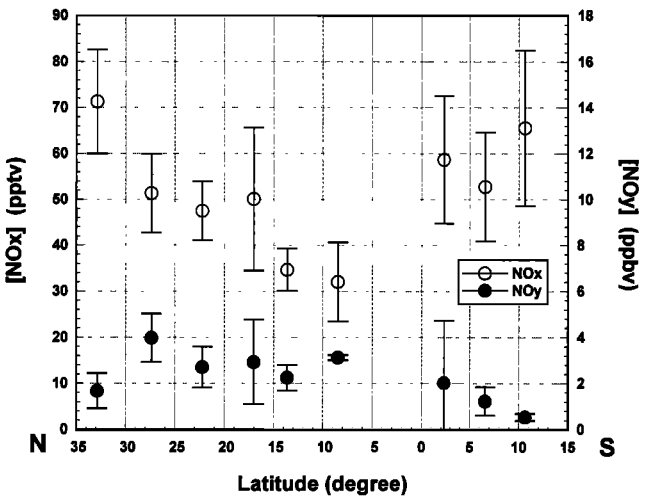

Figure 6*b*. Latitudinal variation in the mean values of NO_x and NO_y. Data have been "binned" into 5° latitudinal increments. Error bars for each mean value reflect the standard deviation for data within the bin. The altitude in all cases is >2.5 km. All data pairs have S/N values >2:1.

environmental data blocks encompass 159 CITE 3 data points out of a total of 190 (S/N > 2:1). The distribution of data over the three major data blocks consisted of FTNH (60), FTTNH (27), and FTSH (72).

The impact of subdividing the total data set into northern and southern distributions is illustrated here in the form of Figure 8. This figure shows a distribution plot of R_E/R_C values based on all non-plume CITE 3 NO-NO_2 data pairs having S/N values of ≥3:1. In this plot the color coded northern hemispheric data clearly show a disproportionately large number of elevated R_E/R_C values. From these data the northern and the southern hemispheric median R_E/R_C values were estimated at 2.3 and .97, respectively.

Still another interesting feature of the northern hemispheric data block is the fact that the trend in R_E/R_C values shows a major discontinuity just to the south of 15°N, increasing from an average value of 2 to a value of ~3 (see Figure 6a). It was this trend, in fact, that suggested that the northern hemisphere database should be examined as two independent data sets. From meteorological data it now appears that one of the major factors involved in this discontinuity was a major change in meteorological conditions during transit flights 11A and 11B. As discussed by *Shipham et al.* [this issue], for the first transit leg the 5-day isentropic back trajectories show that for virtually the entire high-altitude portion of the mission the air flow was from the north/northwest and had originated over the US mainland from points ranging from the Carolinas to Maine. The synoptic picture preceding this outflow was one in which considerable frontal activity and heavy showers were prevalent for several days over large areas of the midwest, Great Lakes, and northeastern United States. This suggests that the air mass sampled during most of flight 11A could best be labeled as "continental outflow." Based on the reported level of convective activity it also appears that this outflow may have had a significant signature of ground level trace gas sources imprinted on it.

Concerning atmospheric conditions to the south of 15°N, the air trajectories indicate that the air mass type changed as the island of Puerto Rico was approached. Near the very end of flight 11A and for the entirety of flight 11B the back trajectories indicate that one component of flow was coming from the east, tropical Atlantic maritime air; and a second component was moving northward from northern South America and could best be defined as tropical continental air. The South American component could not be completely characterized due to limited meteorological data, but indications are that this air also had been significantly influenced by convective activity during the time period of the mission [*Shipham et al.*, this issue]. An examination of the ancillary chemical measurements (Figures 6*a*-6*b*) also shows a significant upturn in the levels of both CO and NO_y and a very sharp drop in O_3 during flight leg 11B. As noted earlier, the calculated R_E/R_C values increased very abruptly during flight 11B, reaching values 1½ to 2 times higher than those observed during flight 11A.

The R_E/R_C values for both northern hemispheric data subsets are summarized in Table 2. From these results it can be seen that the FTNH data (latitude 15° → 35°N) gave a median R_E/R_C value of 1.69 and a mean of 1.74 ± 0.07 (standard deviation of mean) (SDOM), whereas the R_E/R_C median for the FTTNH data (latitude 7° to 15°N) was 2.79 and had a mean value of 3.0 ± 0.24 (SDOM). The corresponding mean R_E values for the northern hemispheric data blocks were 2.37 and 3.73, respectively. The R_E/R_C values cited were based on S/N filtered data at ≥ 3:1 for the FTNH data set and > 2:1 for the FTTNH data. The decision to use only ≥ 3:1 S/N data in analyzing the FTNH data block was based on a more detailed analysis of both the FTNH and the FTSH data subsets. The latter analysis showed an ~40% systematic difference in the mean value of R_E/R_C for data in the range of 2< S/N < 3 versus data having S/N values ≥ 3:1, the former being lower. Thus to optimize the quantitative comparison of observations with theory, we have whenever

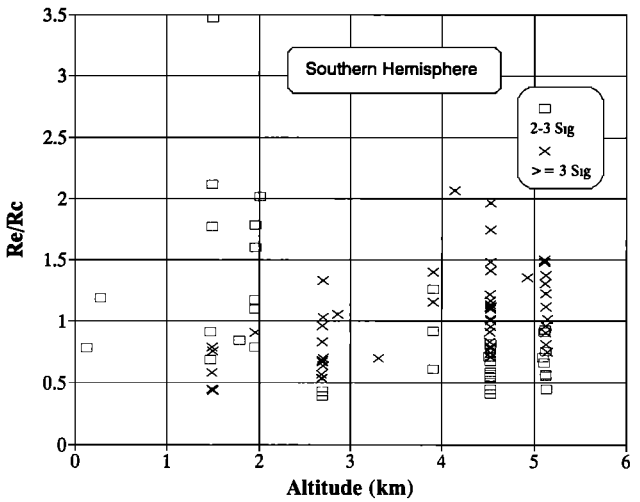

Figure 7*a*. Scatter plots of R_E/R_C versus altitude in the southern hemisphere. Open squares represent data points associated with NO and NO_2 measurements having S/N filtered data in the range 2:1 to 3:1. Crosses represent data having S/N filtered data ≥ 3:1. All "plume" data have been removed.

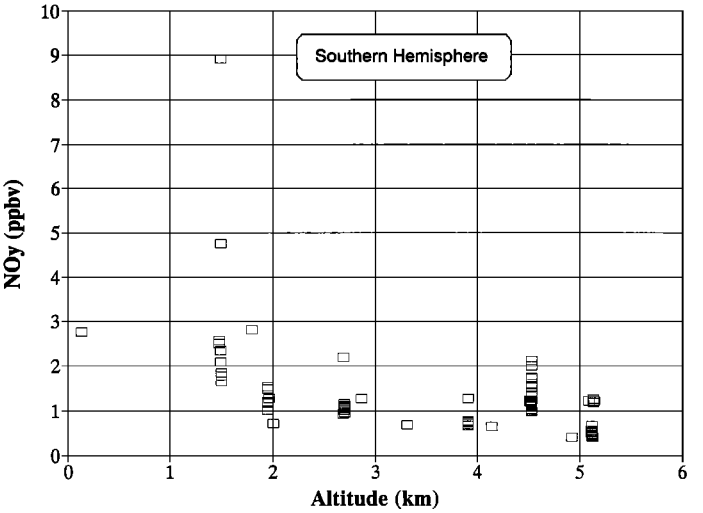

Figure 7*b*. Scatter plots of NO_y versus altitude in the southern hemisphere. All data pairs have S/N value >2:1. All "plume" data have been removed.

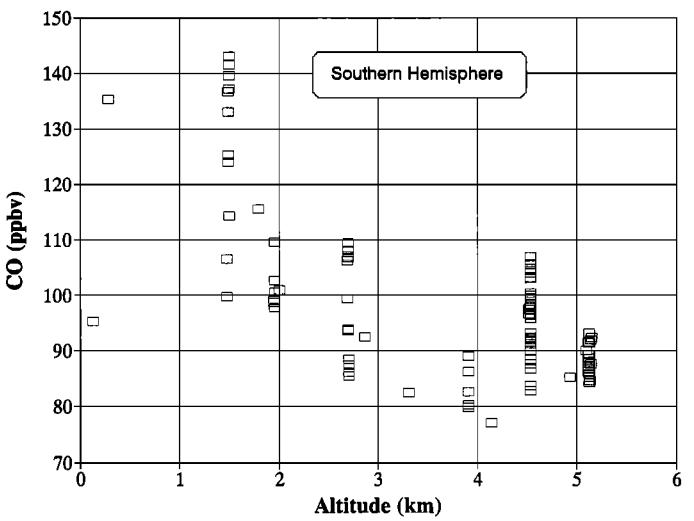

Figure 7*c*. Scatter plots of CO versus altitude in the southern hemisphere. All data pairs have S/N value >2:1. All "plume" data have been removed.

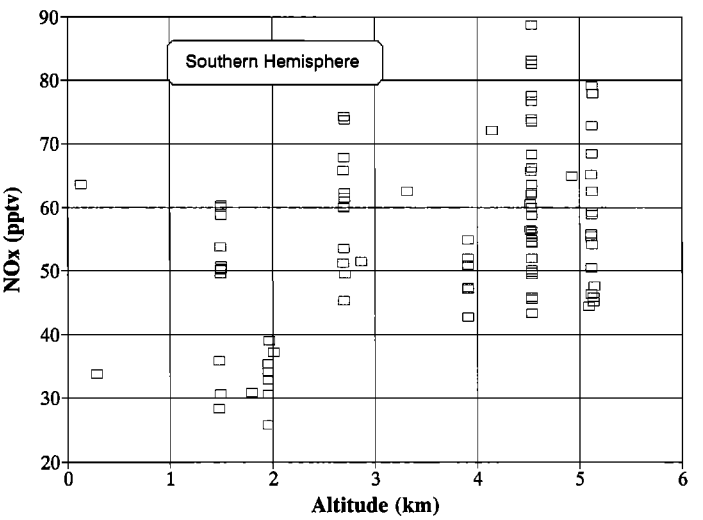

Figure 7*d*. Scatter plots of NO_x versus altitude in the southern hemisphere. All data pairs have S/N value >2:1. All "plume" data have been removed.

possible restricted our analysis to those data having S/N ≥ 3:1. In the case of the FTTNH data set, only six data points were available at S/N ≥ 3:1; and thus no further analysis was carried out at this level.

As discussed previously in the text, the expected median value for the ratio R_E/R_C (i.e., both theory and observations being error free) would be unity. Based on this criterion, it can be seen that for both northern hemispheric data subsets there is very substantial disagreement between model predictions and observations.

In contrast to the northern hemisphere, the southern hemispheric data subset, FTSH, showed very good agreement between model predictions and observations (see Table 2). The median and mean values of R_E/R_C for this data block were 0.97 and 1.01 ± 0.04 (SDOM), respectively. The corresponding mean value for R_E was 2.44. In sharp contrast to the meteorological picture presented for the northern hemisphere, the southern hemispheric picture was relatively simple for the altitude range of 2.5 to 5.5 km. The 5-day isentropic back trajectories indicate that the air mass sampled had originated in the eastern South Atlantic. Although these trajectories do appear to intersect the continent of Africa, the transit time to Brazil is estimated to be of the order of 5 to 9 days. Thus the general meteorological picture for the southern hemispheric component of CITE 3 suggests that a very well aged air mass was sampled. This picture also appears to be in concert with the midaltitude southern hemispheric NO_y

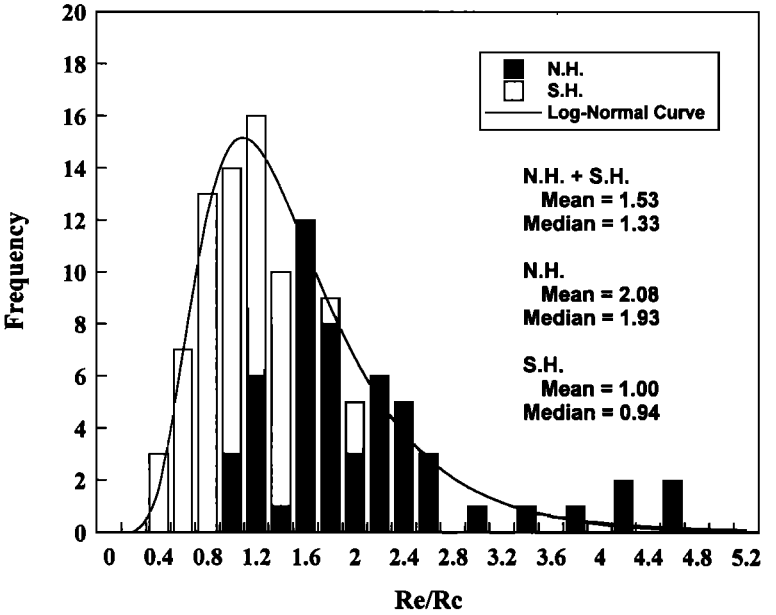

Figure 8. R_E/R_C frequency distribution plot based on S/N data filtering at the ≥3:1 level. The continuous lognormal curve was generated using the log-tansformed mean and standard deviation of the data set. Colored bars indicate the northern hemispheric distribution. All "plume" data have been removed.

measurements which show that the FTSH data had significantly lower NO_y mixing ratios than its northern hemispheric counterpart.

Earlier in the text the potential usefulness of scatter plots involving the quantities $(NO_2)_{Expt}$ and $(NO_2)_{Calc}$ were discussed in the context of qualitatively assessing whether a given photochemical database was "well behaved." Recall that when the entire CITE 3 database was examined in this manner, the binned data gave a Pearson r^2 value of only 0.30. By contrast, the two largest data subsets show very strong correlations between $(NO_2)_{Expt}$ and $(NO_2)_{Calc}$. For example, the FTNH database even though showing one of the largest discrepancies between theory and observation, gave one of the highest r^2 values for any of the regional data blocks, i.e., 0.96 (see Figure 9*a*). Our

Table 2. Summary of R_E/R_C Results for Several Regional Environmental Settings

Regional Environmental Setting and Data Filter Level	Total Points	Total[a] Outliers	R_E	R_E/R_C				[b]Pearson r^2
				MEDIAN	MEAN	SD[e]	SDOM[f]	
Expanded Photostationary State Equation								
FTNH-3S	44	4	2.37	1.69	1.74	0.45	0.07	0.96
FTTNH-2S	27	2	3.73	2.79	3.00	1.20	0.24	0.55
FTSH-3S	49	2	2.44	0.97	1.01	0.29	0.04	0.83
TMBL(P)-5S[c]	10	0	3.71	0.99	1.04	0.33	0.10	0.92
TMBL(P)-5S[d]	10	0	3.71	0.91	0.94	0.28	0.09	0.92
Simple Photostationary State Equation								
FTNH-3S	44	4	2.37	2.39	2.51	0.82	0.13	0.96
FTTNH-2S	27	2	3.73	5.70	6.87	4.13	0.83	0.52
FTSH-3S	49	2	2.44	1.17	1.23	0.39	0.06	0.79
TMBL(P)-5S[d]	10	0	3.71	1.56	1.70	0.73	0.23	0.90

FTNH, free-troposphere northern hemisphere; FTTNH, free-troposphere tropical northern hemisphere, FTSH, free-troposphere southern hemisphere; TMBL(P), tropical marine boundary layer-(plume); 2S, S/N ≥ 2:1; 3S, S/N ≥ 3:1; 5S, S/N ≥ 5:1.

(a) All rejection of outliers was based on a confidence level of 97% or higher.

(b) $(NO_2)_{Calc}$ versus $(NO_2)_{Expt}$.

(c) Hydrocarbon level 1 - Equivalent C_3H_8 - 2.5 ppbv.

(d) Hydrocarbon level 3 - Equivalent C_3H_8 - 25 ppbv.

(e) Standard deviation.

(f) Standard deviation of the mean.

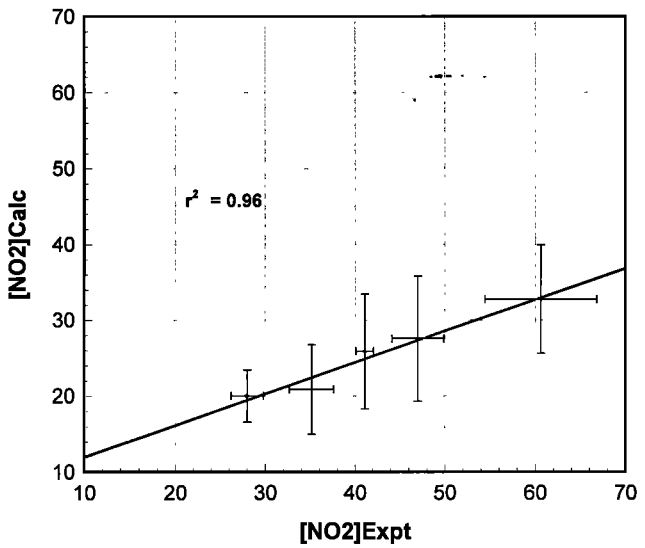

Figure 9*a*. Regression plot of observed NO_2 mixing ratio versus model-calculated NO_2 mixing ratio for the Free Troposphere Northern Hemisphere (FTNH) data subset. Database consists of all NO-NO_2 data pairs having S/N ≥3:1. All "plume" data excluded. Data points have been divided into five bins having an equal number of data points per bin.

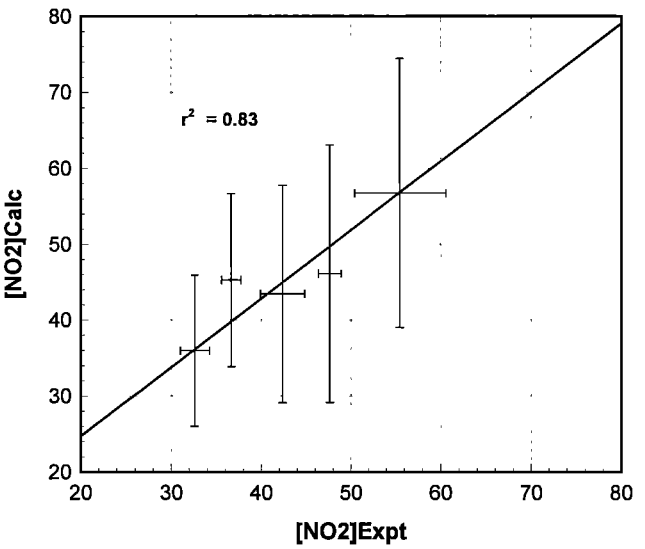

Figure 9*b*. Regression plot of observed NO_2 mixing ratio versus model-calculated NO_2 mixing ratio for the Free- Troposphere Southern Hemisphere (FTSH) data subset. This database consists of all NO-NO_2 data pairs having S/N ≥3:1. All "plume" data excluded. Data points have been divided into five bins having an equal number of data points per bin.

interpretation of this r^2 value is that the major factors influencing $(NO_2)_{Expt}$ were very similar for all NO-NO_2 data pairs within the FTNH data set and that most of these factors also influenced the model evaluated quantity $(NO_2)_{Calc}$. However, the value of R_E/R_C for this data set indicates that the degree of influence of each factor on $(NO_2)_{Expt}$ versus $(NO_2)_{Calc}$ must have been significantly different. As shown in Figures 9*b* and 9*c*, the other two high-

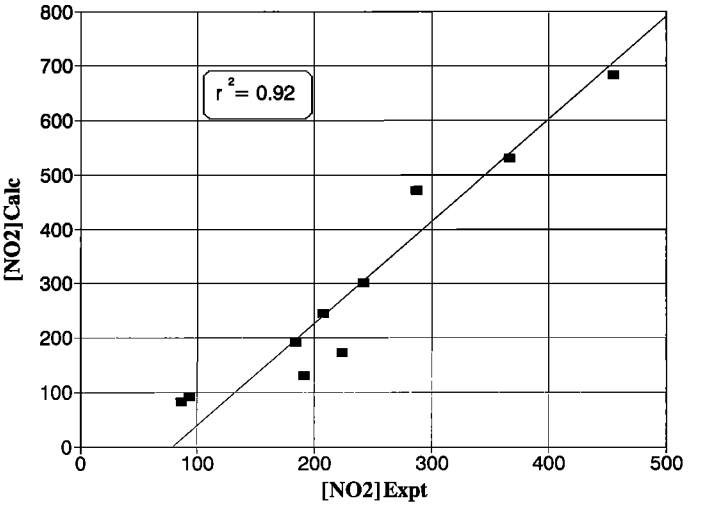

Figure 9*c*. Regression plot of observed NO_2 mixing ratio versus model-calculated NO_2 mixing ratio for the Tropical Marine Boundary Layer (Plume)TMBL(P) data subset. All data pairs have S/N ≥5.

quality data sets, FTSH and TMBL(plume), also gave very large Pearson r^2 values, e.g., 0.82 and 0.92, respectively. Since the R_E/R_C mean values were also approximately unity, we would argue that in these two cases the degree of influence of each photochemical factor on $(NO_2)_{Expt}$ and $(NO_2)_{Calc}$ were quite similar.

Table 2 shows also the R_E/R_C values calculated from equation (1). These results reflect the degree to which "simple theory" can be used to explain the CITE 3 NO-NO_2 observations. In every case, the R_E/R_C values are seen to be significantly higher than those given by equation (2). In fact, with the exception of the FTSH data the difference between "simple" and "expanded" theories equalled or exceeded a factor of 1.5. Thus the substantial difference between the R_E/R_C results from "simple" versus "expanded" theory demonstrate the important role peroxy radicals played in defining the regional photochemical environment of the CITE 3 database. This point is further illustrated in Table 3 where the percentage of the total conversion of NO to NO_2 contributed by peroxy radicals is given. These results indicate that the peroxy radical contribution ranged from 17% to 48%, with the northern hemispheric data defining the middle to high end (e.g., 29% to 48%) and the southern hemispheric, FTSH, data the low end (e.g., 17%). The difference between hemispheres reflects the higher average mixing ratio of O_3 for the FTSH versus the FTNH database (e.g., 50 versus 75 (ppbv)) as well as the lower average UV flux for the FTSH data block (e.g., $J(O^1D) = 1.99 \times 10^{-5}$, FTSH, versus 3.78×10^{-5}, FTNH). For both regions it was generally found that the most important of the peroxy species was HO_2 (~50%), followed by CH_3O_2 (~27%) and RO_2 (~23%). Total peroxy radical, PO_2, mixing ratios for high Sun conditions ranged from 30 to 60 pptv both for the FTNH and the FTSH data sets.

In addition to the three major data blocks, two smaller data subsets also were defined. Each involved a uniquely different chemical environment. These smaller databases involved the

TABLE 3. Summary of Peroxy Radical Contributions in the Conversion of NO to NO_2

		$k_a[PO_2]/\{k_a[PO_2]+k_1[O_3]\}$			$k_4[HO_2]/k_a[PO_2]$		
Data Set	Points	Avg, %	Min, %	Max, %	Avg, %	Min, %	Max, %
FTNH	40	29	14	46	56	43	66
FTTNH	25	48	15	66	41	31	54
FTSH	47	17	6	37	53	38	62
TMBL(P)HC-3	10	41	26	53	47	35	59
TMBL(P)HC-1	10	36	22	46	59	46	71
		$k_5[CH_3O_2]/k_a[PO_2]$			$k_6[RO_2/k_a[PO_2]$		
Data Set	Points	Avg, %	Min, %	Max, %	Avg, %	Min, %	Max,
FTNH	40	28	23	40	17	4	23
FTTNH	25	36	27	49	23	8	28
FTSH	47	25	22	33	22	16	36
TMBL(P)	10	22	17	27	31	24	38
TMBL(P)	10	27	19	37	14	9	22

HC-1, hydrocarbon level 1 (equiv. C_3H_8 = 2.5 ppbv); HC-3, hydrocarbon level 3 (equiv. C_3H_8 = 25 ppbv). Avg k values: $k_a=8.9\times10^{-12}$; $k_4=9.1\times10^{-12}$;$k_5=8.1\times10^{-12}$; $k_6=8.9\times10^{-12}$. $[PO_2] =[HO_2] + [CH_3O_2] + [RO_2]$.

trade wind inversion in the southern hemisphere (TWISH), and the tropical marine boundary layer as observed off the island of Puerto Rico TMBL(P).

The trade wind inversion database is made up of very limited data (e.g., 18 data points) most of which have low S/N ratios, e.g., $2 \leq$ S/N ≤ 3. As shown in Figure 7*a* these low S/N data resulted in widely varying R_E/R_C values, ranging from 3.5 to 0.4; thus they do not lend themselves to a meaningful quantitative interpretation.

In contrast to the TWISH database, we believe that the data block labeled TMBL(P) does merit further comment. In this case, even though the database is weak in terms of numbers (i.e., only 10 data points), the highly elevated mixing ratios for NO and NO_2 produced data pairs having an average S/N ratio of nearly eight. Based on assumed hydrocarbon levels of 25 and 5 ppbv of equivalent C_3H_8 (i.e., see Tables 1b and 2), the median values for R_E/R_C were calculated at 0.91 and 0.99, respectively; the corresponding mean values for this data subset were .94 $\pm$ 0.09 and 1.04 $\pm$ 0.10 (SDOM), respectively. Thus even though the data are very limited, one may draw the tentative conclusion that for "moderate" mixing ratios of NO_x (100 to 500 pptv) tropical-marine boundary layer chemistry is well represented by equation (2). An interesting aspect of the TMBL(P) data subset was the observation that the NO_y mixing ratio during this data run ranged from a low of 6 ppbv to a high of 10 ppbv. In spite of these high levels of NO_y, it appears that they resulted in no interference in the measurement of NO_2 (see discussion later in text).

For reader convenience we have summarized all data subset acronyms and their respective regional environmental descriptions in Table 4.

ASSESSMENT OF ERRORS AND DISCUSSION

Based on the highest S/N filtered data summarized in Table 2, it can be seen that there are two data subsets in which model predictions and experimental observations are consistent and two where the agreement is quite poor. As discussed earlier in the text, there also was one data subsets (e.g., TWISH) that had so few data pairs at S/N values of $\geq$3:1 as to render the final results of very limited value. Data subsets showing a high level of agreement between theory and observation are those labeled here as TMBL(P) and FTSH, whereas significant disagreement is seen in the two northern hemispheric data sets, i.e., FTNH and FTTNH. To gain further insight concerning the large R_E/R_C bias in the northern hemispheric data, three questions were explored: (1) How does the magnitude of disagreement compare with the magnitude of the random and systematic errors associated with the analysis? (2) What are the major chemical and physical differences between those databases showing poor agreement versus those in good agreement with model predictions? (3) Based on the findings from questions 1 and 2, what conclusions may be drawn concerning possible shortcomings in the CITE 3 measurements versus shortcomings in our model description of the NO-NO_2 photochemical system?

Given that the FTNH data set was the most robust data subset of the two data subsets showing a high R_E/R_C bias, it served as the principal focus of our investigation of questions 1-3. To proceed with this analysis, however, further reflection is required on defining the "reference point" for the ratio R_E/R_C. Recall that earlier in the text for the case where the ratio of two lognormal

TABLE 4. CITE 3 Data Subsets

Environmental Regime	Acronym	Geographical Coordinates
Free-tropospheric northern hemisphere	FTNH	19.4°-35.0°N 67.0°-74.6°W
Free-tropospheric southern hemisphere	FTSH	11.1°-0.0°S 30.0°-49.5°W
Free tropospheric tropical northern hemisphere	FTTNH	6.8°-16.3°N 54.1°-63.0°W
Trade wind inversion southern hemisphere	TWISH	10.0°-2.5°S 28.2°-33.6°W

distributions (i.e., R_E/R_C) was examined, the "reference point" for perfect agreement between observations and model predictions was defined in terms of the median where the expected median value was unity. Thus significant deviation from unity was used as the basis for demonstrating the level of disagreement between observations and model predictions. Even so, it is quite apparent that the median does not readily lend itself to a quantitative assessment of the level of disagreement in the same way that the arithmetic mean does for the case of a normal distribution. In the special case , however, where the coefficient of variation (e.g., standard deviation/mean) is $\leq 1/3$ for a lognormal distribution, from a practical point of view, normal statistics may be used to quantitatively analyze the lognormal distribution [*Hald,* 1962]. Under the above conditions, the expected median is unity and the expected mean is also closely approximated by unity. As seen from Table 2, all data subsets but FTTNH satisfy or closely approximate the condition given above. Further evidence supporting this position can be found in the mathematical closeness of the median and the mean for the FTNH, FTSH, and TMBL(P) databases where the agreement is seen to be within 5%. Given, then, the statistical conditions described above, the analysis that follows will be based on the use of the arithmetic mean.

Concerning question (1) which addresses the issue of random and systematic errors, it can be seen from Table 2 that, based on a S/N filter of $\geq$3:1, the FTNH data gave a mean R_E/R_C value of 1.74. The estimated SDOM for this data subset was $\pm$ 0.07. For all data sets analyzed here, it is the standard deviation of the mean (SDOM) that will be used to define how well the mean is known. In this case, the mean R_E/R_C value is over 10 σremoved from that predicted by equation (2). To assess the relative contributions of R_E and R_C to the random error associated with R_E/R_C, a propagation of error analysis was performed on the basic equation $R = R_E/R_C$. In our analysis all 40 (S/N $\geq$3:1) NO-NO_2 FTNH data pairs were evaluated. These results showed that the relative error in R_C (e.g., $\Delta R_C/R_C$) was 20% and that for R_E was 35%. Thus when added in quadrature, the relative contribution of R_C and R_E to the total uncertainty in the ratio R_E/R_C was 25 and 75%, respectively. These results indicate that the uncertainties associated with the measurement of NO_2 and NO were the major sources of random error in the evaluation of the ratio R_E/R_C.

In the context of question (1), the potential importance of systematic errors was also explored. Systematic errors can arise both due to errors in the measurements of individual physical and chemical variables used in the overall evaluation of R_E/R_C (e.g., NO_2, NO, O_3, UVZ, UVN, CO, H_2O, NMHC, T, and P) or due to errors in the many photochemical and gas kinetic rate constants used in modelling calculations. In the latter case, it is important to recognize that it doesn't matter whether the error in a "J" or "k" coefficient has been caused by a random or systematic error in some experiment used to determine its value. Since the sign of the error does not change from one run to another, it always manifests itself as a systematic error in the model output and therefore in the value of R_C.

In assessing the resultant systematic error from the "J" and "k" values used in our calculations, we have employed a Monte Carlo procedure similar to that presented by *Thompson and Stewart* [1991]. In our evaluation the estimated errors in all "J" and "k" values are those given by [*Demore et al.* 1992]. The errors were assigned a lognormal probability distribution for values that must be positive, and normal distributions were assigned to errors for values that could be either positive or negative. In our analysis an average temperature of 273 K was used for the FTNH data in randomly producing 1000 independent sets of "J" and "k" values. Based on a representative data point from the FTNH environment, calculations were then carried out for each set of "J" and"k" values. The output from these calculations gave probability distributions for the systematic error due to "J" and "k" in the model results. For example, the probability distribution for R_E/R_C had a standard deviation of 0.64. While the true systematic error is unknown, an error the magnitude of one standard deviation does shift the original FTNH mean value of 1.74 to 1.1 (e.g., 86% of the bias is removed). Although this might be viewed as an encouraging result, it raises the obvious difficulty that all other data subsets would have to be corrected by approximately the same percentage (e.g., 37% of the initial R_E/R_C value). Quite clearly, the application of this magnitude of

correction to the FTSH and TMBL(P) data would result in an unacceptably large negative bias in the R_E/R_C mean values for these databases. This suggests that the actual magnitude of the systematic error in R_E/R_C, associated with the J and k values, is most likely significantly smaller than that cited above. If so, a major component of the FTNH R_E/R_C bias would remain.

Concerning possible systematic errors in the observational data, the situation here is more complex than that involving the J and k uncertainties. Part of this complexity arises from the fact that for airborne-observational field data a given systematic error may affect the data recorded all of the time and therefore be viewed as stationary throughout the data set, or it may appear only under very specific conditions in which case the sign of the error may be known but the magnitude would vary in time. Thus the latter type of error may apply to only one segment of an overall data set. As discussed in the text above, a stationary type systematic error cannot resolve the discrepancy between the FTNH and the FTSH data subsets.

To assess the possible effects of variable systematic errors, we have examined both the FTNH and FTSH data in terms of their respective critical chemical and physical parameters. We have defined a "critical" parameter in this case as one whose value would have a near 1:1 linear effect on the value of R_E/R_C. Thus given that it satisfied the criteria of being nonuniform in its impact on the FTNH and FTSH databases, a "critical" parameter would lead to a correction in the R_E/R_C values for the FTNH data without a concomitant adjustment in the R_E/R_C values of FTSH.

To identify these "critical" parameters, sensitivity calculations were performed on all four data subsets. The results are shown in Tables *5a* and *5b*. For these calculations, R_E/R_C values were estimated for independent changes in each of the listed test variables (e.g., H_2O, CO, O_3, NO, NO_2, UV(zenith), and UV(nadir)) where each test variable was adjusted in value in stepwise increments which ranged up to a factor of $\pm$ 2. The calculations were performed on a single representative run from each data subset that had an R_E/R_C value close to the mean value for that database. For the hydrocarbon sensitivity tests, the original hydrocarbon level was decreased by a factor of 2.0 but increases in hydrocarbon levels were carried out by adding the surrogate hydrocarbon species toluene in 2.0 ppbv steps (see discussion below for details).

The results from these calculations indicate that the "critical" parameters in the evaluation of R_E/R_C are O_3, NO, NO_2, UV(zenith), and (non-methane hydrocarbons) (NMHCs). As related to the FTNH and FTSH databases, the discussion that follows is focused on examining whether significant systematic errors may have been present in one of the above parameters for one data subset but not the other.

Concerning the "critical" species O_3, we found no evidence in the data themselves nor anything recorded in flight books that

TABLE *5a*. Model Sensitivity Calculations: H_2O, CO, O_3, NO, NO_2 and UV

Data Set	Change Factor	R_E/R_C Values						
		H_2O	CO	O_3	NO	NO_2	UV-Z	UV-N
FTNH	0.50	1.76	1.64	2.81	3.24	0.82	1.07	1.51
	0.85	1.68	1.65	1.88	1.93	1.40	1.48	1.61
	1.00	1.65	1.65.	1.65	1.65	1.65	1.65	1.65
	1.15	1.62	1.65	1.47	1.44	1.90	1.81	1.69
	2.00	1.52	1.66	0.92	0.84	3.31	2.68	1.93
FTTNH	0.50	3.02	2.57	4.28	5.08	1.33	1.77	2.50
	0.85	2.74	2.63	2.98	3.09	2.25	2.41	2.61
	1.00	2.65	2.65	2.65	2.65	2.65	2.65	2.65
	1.15	2.58	2.67	2.40	2.33	3.05	2.89	2.70
	2.00	2.27	2.74	1.57	1.39	5.32	4.07	2.95

TABLE *5b*. Model Sensitivity Calculations: Hydrocarbon

Data Set	R_E/R_C Values				
	0.5 * HC	1.0 * HC	HC+2	HC+4	HC+9
FTNH	1.69	1.65	1.20	1.06	0.94
FTTNH	2.77	2.65	1.56	1.35	1.20
FTSH	1.01	0.98	0.81	0.74	0.67
TMBL(P)	0.83	0.79	0.66	0.60	0.54

0.5*HC, fraction of original HC level. HC+2, HC+4, and HC+9, surrogate hydrocarbon (e.g., toluene) additions to original hydrocarbon mix in parts per billion by volume.

suggests that there were any problems in the performance of this instrument. Similarly, an evaluation of the critical parameter UV(zenith) indicated that this parameter was an unlikely source of systematic error. Flight notes gave no indication of any failure in this instrument during the mission nor was there any indication of any significant shift in the instrument's calibration factor as measured by the Eppley Company before and after the CITE 3 mission. Recall however, that the major use of the UV(zenith) measurement in our analysis was to correct our two-stream model J values for overhead clouds and haze. In combination with the UV(nadir) measurement, these two parameters produced what we earlier defined as the "cloud correction factor" (CCF), see model description. For purposes of this evaluation, therefore, we examined the FTNH and FTSH data to see if there were any major differences in CCF values. The results from this inspection revealed that the average $J(NO_2)$ and CCF values for the FTNH data set were 0.0105 and 1.13, respectively, and those for FTSH were 0.0084 and 1.04, respectively. Thus as was the case for O_3, the UV(zenith) results do not appear to explain any of the R_E/R_C difference between the two databases.

Values for the third "critical" variable, NO, are those derived from LIF measurements. As discussed earlier in the text, this measurement technique should have been relatively free of any artifacts since the two-photon spectroscopic specificity of this methodology renders it virtually free of chemical interferences. (Both laboratory and airborne field tests have so far corroborated the latter point of view [*Bradshaw et al.*, 1985; *Davis et al.*, 1987]). The very high sensitivity for detection of NO (i.e., detection limit of 3 pptv) and the periodic in-flight standard addition calibration of this system also suggests that the level of systematic error in these measurements should have been negligibly small. An examination of the FTNH and FTSH data sets, show that very similar mixing ratios for NO were observed in both hemispheres, e.g., FTNH, NO_{Avg} = 20 pptv, and FTSH, NO_{Avg} = 22 pptv.

Unlike NO, the measurement of NO_2 does present the possibility of a variable systematic error. The reason for this lies in the fact that the measurement of NO_2, unlike NO, is not a direct measurement. As discussed earlier in the text, the NO_2 measurement involves the initial step of photofragmentation ($NO_2 + h\nu \rightarrow NO + O$), followed by the two-photon LIF detection of the NO photofragment. Thus to the extent that an unknown/unidentified NO_y species (i.e., some form of organic nitrate) undergoes photolytic decomposition and produces NO_2 as a product, this NO_2 photofragment would lead to a signal indistinguishable from that derived from natural NO_2. Alternatively, any NO_y species that has a high rate of decomposition on surfaces or that could thermally decompose in the gas phase to form NO_2 (e.g., N_2O_5, HO_2NO_2, PAN) also would have the potential for creating an interference problem. The importance of the latter source increases as the sample residence time becomes long and/or there are significant differences in the sample chamber temperature relative to the ambient outside air temperature. As configured during CITE 3, the PF-LIF NO_2 instrument used a continuum light source that was filtered to restrict the photolysis wavelength from 350 to 410 nm. This relatively narrow bandwidth centered at long wavelengths most likely eliminated most NO_y species from becoming a problem. In addition the sample residence times were kept very short (i.e., 2 to 4.5 s), and the sample inlet lines were maintained within a few degrees of the outside air temperature. Tests by Georgia Tech investigators using known amounts of HNO_3 and a limited number of alkylnitrates and nitroalkanes also suggest the absence of interferences from these classes of compounds [*Sandholm et al.*, 1990, 1992]. On the other hand, when the sum of individually measured NO_y compounds, as recorded in other airborne field programs, is compared against total measured NO_y, very frequently a "shortfall" has been found in the budget. This suggests that there are still several NO_y compounds that remain unidentified [*Hubler et al.*, 1992; *Singh et al.*, 1993; *Ridley*, 1991; *Sandholm et al.*, 1992, 1993]. Of the known but yet unmeasured NO_y species, the labile compounds HO_2NO_2 and N_2O_5 could perhaps present the most serious problem. These compounds, in addition to their thermal decomposition in the gas phase, could very well undergo rapid decomposition on surfaces. For both of these compounds NO_2 would most likely be one of the decomposition products.

The issue of NO_y interference in the measurement of NO_2 is centrally important to this analysis since a comparison of the FTNH and FTSH NO_y data (e.g., see Figure 6*b*) indicates a considerable difference in the NO_y mixing ratios for these two data subsets. For example, the FTNH data show NO_y mixing ratios ranging from 0.9 to 6.2 ppbv with an average value of 2.5 ppbv. By contrast, the FTSH data gave an average NO_y mixing ratio of 1.1 ppbv with a range of 0.4 to 2.1 ppbv.

Although the potential effect of NO_y on the FTNH R_E/R_C bias is difficult to quantify, some insight can be gained concerning the relative magnitude of this problem in comparison to the FTSH database. For example, the two most critical factors that might be expected to influence the level of interference are the absolute NO_y concentration levels and the chemical composition of NO_y in each environment. The chemical composition could have been different either because the two environments had quite different NO_y sources and/or because they had quite different ambient temperatures. For example, NO_y species such as peroxy acetylnitrate (PAN) typically are present at mixing ratios of only a few pptv in the TMBL but may be present at well over 100 pptv at high altitudes [*Singh et al.*, 1990, 1992; *Ridley et al.*, 1990]. Similar temperature stability considerations apply to species like N_2O_5 and HO_2NO_2. As related to the FTNH and FTSH data sets the relative difference in NO_y composition due to temperature effects would appear to be minor. In this case, the average temperature for the FTNH data was 275 K and for FTSH 276 K; equally important, the temperature ranges for these databases (e.g., 271-278 K and 269-285 K, respectively) were also quite similar.

Given the above findings, we have further explored the NO_y interferant hypothesis by examining the FTNH data set in terms

of scatter plots involving the parameters NO_y, R_E/R_C, temperature, and other related variables. The working hypothesis here has been that if the highest NO_y levels provided a significant source of interferant NO_2, $(NO_2)_{Interf}$, then one might expect a significant correlation between the magnitude of NO_y and the magnitude of the difference between $(NO_2)_{Expt}$ and $(NO_2)_{Calc}$. In this scenario, $(NO_2)_{Expt}$ would be defined by the sum $(NO_2)_{True}$ + $(NO_2)_{Interf}$. The results from the first of these analyses involving "binned" R_E/R_C and NO_y data is shown in Figure 10. In this case the Pearson r^2 value is estimated at 0.03. The latter value would thus suggest that the interference level from NO_y was of only secondary importance in explaining the FTNH bias. However, because NO_y at middle free-tropospheric altitudes is typically dominated (e.g., 50 to 75%) by the concentration levels of HNO_3, PAN, and NO_x [*Singh et al.*, 1990; *Ridley et al.*, 1990; *Sandholm et al.*, 1992, 1993], it also could be argued that "total" NO_y may not be the best choice as the independent variable for a regression analysis. The authors note, for example, that both in laboratory tests and in detailed analysis of field data, neither HNO_3 nor PAN have surfaced as major NO_2 interference sources when NO_2 photoconverters have been used and the photoconverter has had appropriate spectral filtering. The latter observations suggest that perhaps a more meaningful scatter plot might be ΔNO_y versus R_E/R_C, where $\Delta NO_y = NO_y - (HNO_3 + PAN + NO_x)$. Unfortunately, during the CITE 3 mission, neither HNO_3 nor PAN were measured, thus precluding our exploring this possibility.

Still another consideration in our assessment of the NO_y-NO_2 interference hypothesis was the possible importance of the ratio NO_y/NO_2. For example, it may be argued that the larger this ratio the higher the probability that even a small percent decomposition of NO_y would have a significant impact on the value of $(NO_2)_{Expt}$. In actual fact, all that is required to shift the observed FTNH R_E/R_C average from 1.74 to 1.0 is an $(NO_2)_{Interf.}$ level of 18 pptv. (Recall the reported average NO_2 mixing ratio for the FTNH data was 42 pptv.) This NO_2 interference level (i.e., 18 pptv) represents less than 1% of the estimated average FTNH NO_y mixing ratio of 2500 pptv. In an effort to explore the latter possibility, a scatter plot was made of R_E/R_C versus NO_y/NO_2; see Figure 11. The results from this binned data plot gave an r^2 value of 0.41. Although more indicative of an interference problem, this modest r^2 value does not convincingly show that $(NO_2)_{Interf}$ from NO_y was the primary source of the FTNH R_E/R_C bias. By contrast, a similar analysis of the FTSH data gave a still lower r^2 value of 0.34.

In a final attempt to gain further insight into the NO_y interference question, we also examined the possible influence of the highly labile NO_y species HO_2NO_2, per nitric acid. The concentration of this species is defined by the thermal equilibrium

(R7) $\quad NO_2 + HO_2 + M \leftrightarrow HO_2NO_2.$

As shown in Table 6, for the average temperatures reported for the FTNH and FTSH data sets, the estimated mixing ratio for HO_2NO_2 is ~2 pptv and therefore should have been of little consequence as an interference. However, within the 1σ error bar given for the equilibrium constant for this species, its mixing ratio could have ranged from a high of 15 pptv to a low of 0.1 pptv. To assess the interference potential of HO_2NO_2, all R_E/R_C values (i.e., S/N $\geq$ 3) from the FTNH database were plotted versus temperature. The argument here would be if HO_2NO_2 were a major source of $(NO_2)_{Interf}$, the lower the temperature the more HO_2NO_2 present and the larger the expected value of R_E/R_C. The results from this regression analysis showed no such correlation. In fact, the reverse trend was found, that is, the value of R_E/R_C was found to increase slightly with increasing temperature. Equally important here is the observation made earlier in the text that the average temperature and average NO_2 levels for both the

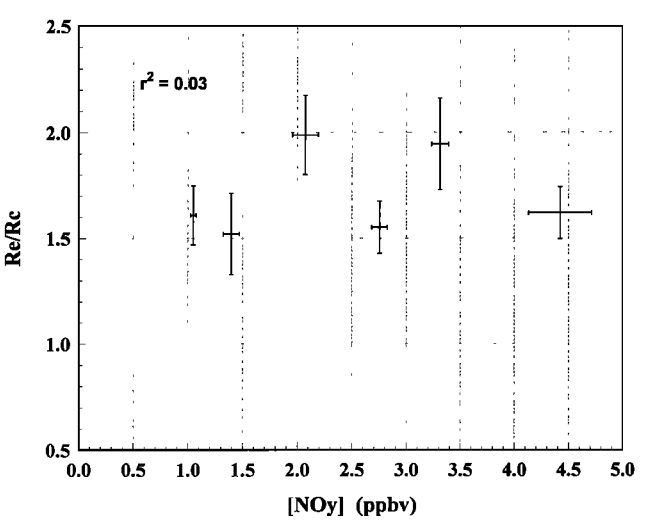

Figure 10. Scatter plot of R_E/R_C versus the observed NO_y mixing ratio. Data set consists of FTNH data pairs having S/N $\geq$3:1. All "plume" data have been removed.

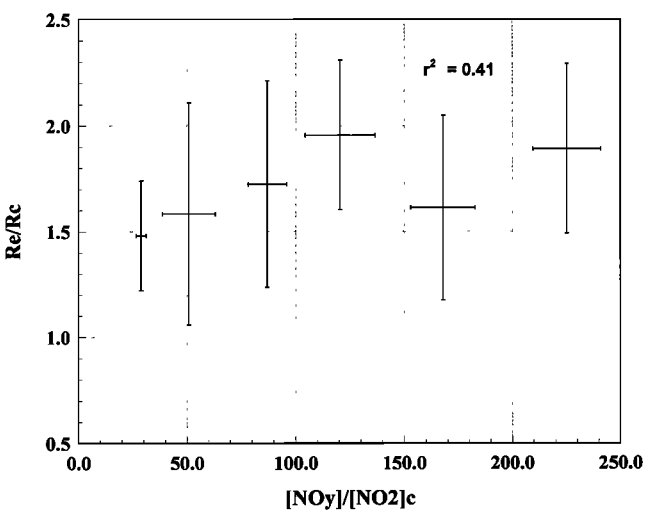

Figure 11. Scatter plot of R_E/R_C versus the ratio $NO_y/(NO_2)_{Calc}$. The data set consists of all FTNH data pairs having S/N $\geq$3:1. All "plume" data have been removed.

TABLE 6. Pernitric Acid (HO_2NO_2) Mixing Ratio as a Function of Temperature

Temp, K	Temp, C	Keq	Uncertainty Factor f	$[HO_2NO_2]$ Best Estimate, pptv	$[HO_2NO_2]$ Min, pptv	$[HO_2NO_2]$ Max, pptv
293	20	3.0×10^{-11}	5.1	0.18	0.04	0.92
288	15	5.7×10^{-11}	5.1	0.34	0.07	1.77
283	10	1.1×10^{-10}	5.2	0.67	0.13	3.51
278	5	2.2×10^{-10}	5.3	1.34	0.25	7.14
273	0	4.6×10^{-10}	5.4	2.76	0.51	14.9
268	-5	9.7×10^{-10}	5.5	5.81	1.06	31.9

Conditions: $[HO_2] = 1.5 \times 10^8$ molecules/cm^3, pressure = 550 mbar; $[NO_2]$ = 40 pptv.

FTNH and FTSH databases were very nearly the same. Under these conditions the HO_2NO_2 impact on R_E/R_C for both data subsets would be expected to be nearly the same.

Based on the above information, it is not possible at this time to clearly identify a specific NO_y interference source that would have a disproportionately larger influence on the R_E/R_C values of the northern hemisphere free tropospheric database. All attempts to correlate some form of an interference parameter with R_E and R_C values produced results that only moderately support the presence of an NO_y/NO_2 interference. On the other hand, the fact that the data themselves are quite noisy, that a large difference exists between the average mixing ratios for NO_y for the two databases (e.g., 2.5 ppbv FTNH versus 1 ppbv FTSH), that there was much greater variability in the FTNH NO_y levels (0.9-6.2 versus 0.4-2.1 ppbv), and the fact that less than a 1% NO_2/NO_y interference (i.e., 18 pptv) could totally remove the FTNH R_E/R_C bias still leaves open the real possibility that the R_E/R_C bias may be totally explicable in terms of the interference hypothesis.

The final "critical" variable identified from our sensitivity analysis as having the potential for a large effect on the value of R_E/R_C was non-methane hydrocarbons (NMHCs). From Table 1*b*, it can be seen that only five hydrocarbon samples were collected during missions 11a and 11b which encompass the FTNH and FTTNH data sets. In general, the analyses of these samples (e.g., $C_2 \rightarrow C_4$) showed that NMHC levels were relatively low, having an integrated reactivity with OH that ranged from 0.76 to 3.88 ppbv equivalent propane (C_3H_8). These low NMHC levels typically had a 10% or less effect on the evaluated R_E/R_C ratios for the FTNH data (see e.g., Table 3). Based on these results, the impact of NMHCs on the R_E/R_C FTNH bias would appear to be quite small. This raises the question, however, whether the five NMHC samples taken during mission 11 were indeed representative of the actual northern hemisphere hydrocarbon environment over the designated flight track (e.g., Figure 1). Evidence suggesting that they were can be seen in the CO data. For example, the northern hemisphere middle-altitude ($z \geq 3$ km) CO data averaged only 90 ppbv, having a maximum value of 115 ppbv. Quite clearly, these CO levels reflect those one would expect to find in a relatively clean environment, i.e., one having been little affected by significant combustion sources. An important aspect of the CITE 3 CO measurements, as related to the question of representative sampling, is that these measurements were recorded continuously using the well established TDL (tunable diode laser) technique. Thus it could be argued that the CO measurements tend to support the contention that the limited number of NMHC grab samples taken during the transit flight were representative of the actual hydrocarbon environment.

Evidence suggesting that atmospheric conditions might have been chemically more complex during the northern hemisphere transit flight can be found in the CITE 3 NO_y measurements and the meteorological data. As discussed earlier in the text, the 5 day back trajectories for the Wallops Island, Virginia, to Puerto Rico transit flight show that the air sampled between 3.6 and 4.8 km (aircraft altitude) had moved off the northeastern and central eastern U.S. coast turned abruptly south (the effects of Hurricane Gabriel) and then moved down through the western Atlantic toward the Caribbean. The estimated time that this air was over the western Atlantic before aircraft sampling, occurred ranges from 1/2 to 3 days (e.g., ranging from the first hour of flight to the end of mission 11A as Puerto Rico was approached). For most of the flight from Wallops Island, Virginia, to Puerto Rico, then the general classification of the air sampled would be "middle-altitude continental outflow." The back trajectories, in combination with synoptic data, also suggest that for 1-3 days before passing over the U.S. coast, the air parcel sampled had experienced extensive convective activity in combination with heavy rain showers [*Shipham et al.*, this issue]. Thus the general overall picture that emerges is one which suggests that there had been extensive mixing of surface sources into midtropospheric air at 3 to 5 km.

The chemical evidence supporting the notion of a more complex middle-altitude chemical environment during the northern hemisphere transit flight involves the reported NO_y measurements. For example, the high average mixing ratios for NO_y, the high degree of variability, and the strong correlation between dew point and NO_y levels (e.g., $r^2 = 0.81$) would seem to be consistent with significant ground level NO_x being transported into the middle troposphere. If the latter were true, however, it also would seem to follow that one should have observed elevated levels of both NMHCs and CO.

A scenario that potentially resolves this apparent conflict would involve the hypothesis that the major source of NO_y was not predominantly ground level combustion but rather lightning. The latter source appears to be compatible with the observed elevated, variable NO_y levels cited above and is also consistent with the high correlation found between NO_y and dew point. Provided that the additional assumption is made that the major component of the convectively transported ground level air was predominantly rural in its composition, it is also consistent with

the CO and hydrocarbon observations. Based on the lightning hypothesis, then, the air sampled during the transit flight at 3 to 5 km would have had elevated levels of NO_y, modest levels of CO, and the hydrocarbon mix would have been more characteristic of biogenic emissions. Unfortunately, as shown in Table 1*b*, the latter type species were not analyzed in the CITE 3 grab samples. However, based on recent results summarized by *Chameides et al.* [1992] for the time period of September, surface isoprene levels as high as 0.7 ppbv could be expected. (The concentrations of propane (C_3H_8) and toluene equivalent in reactivity to this level of isoprene are 70 and 10 ppbv, respectively). These surface levels of isoprene would most likely have been diluted by factors of 4 to 5 due to convective transport to higher altitudes and also would have been further reduced in concentration due to their rapid reaction with OH radicals. Even so, these losses do not preclude the possibility that some mix of unreacted parent hydrocarbon (i.e., isoprene) and reactive oxidation by-products may have provided a source of peroxy radicals that significantly exceeded that which was used in our initial calculations of the ratio R_E/R_C [*Calvert and Madronich,* 1987; *Madronich and Calvert,* 1989, 1990]. In an effort to test this NMHC hypothesis, several hydrocarbon modelling simulations were carried out in which the integrated chemical effect of a reactive hydrocarbon mix was simulated using the surrogate hydrocarbon species toluene. In the first set of simulations, the surrogate species was added to gas mixtures corresponding to specific FTNH runs where the runs chosen had R_E/R_C values close to that of the mean for the entire data set, e.g., 1.74. The results from these simulations are those shown in Table 5*b* and reflect the hydrocarbon sensitivity tests cited earlier in the text. From Table 5*b* one can estimate that at a toluene mixing ratio of 3 ppbv, 80% of the FTNH R_E/R_C bias is removed, reaching a value of 1.15. In fact, for toluene mixing ratios much greater than 4 ppbv, the rate of reduction in the value of R_E/R_C decreases significantly due to the suppression of OH and a subsequent plateauing of the peroxy radical concentration. (Note that based on a diurnally-averaged OH level of 1 x 10^6/cm^3 for middle-altitude conditions, toluene would have an estimated lifetime of approximately 2 days at 275 K.)

At levels of 3 ppbv, the peroxy radical conversion of NO to NO_2 was estimated to be ~50% of the total conversion rate of NO. By contrast, from Table 3 it can be seen that when using the background hydrocarbon mixture for the FTNH data, corresponding to our previously defined level 1 , peroxy radicals accounted for only 29% of the NO to NO_2 conversion rate (level 1 is approximately equivalent to 0.4 ppbv toluene).

Overall, the above results suggest that from a theoretical point of view the addition of a moderately reactive surrogate hydrocarbon to the gas mixture of each sampling run does remove the major component of the R_E/R_C bias in the FTNH data. However, these results raise yet a different question. If such enhanced hydrocarbon mixtures were present, what impact might they have on O_3 (i.e., O_3 tendency), and are these estimates in reasonable agreement with actual O_3 observations? To address this question for the hydrocarbon conditions stated above, the O_3 tendency was evaluated using equation (6):

$$P(O_3) = [NO](k_4[HO_2] + k_6[RO_2]) - k_{10}[O(^1D)][H_2O] - [O_3](k_{11}[HO_2] + k_{12}[OH]) \quad (6)$$

where the new reactions (R9) → (R12) represent the major O_3 destruction processes, e.g.,

(R9) $O_3 + h\nu \rightarrow O(^1D) + O_2$

(R10) $O(^1D) + H_2O \rightarrow 2\ OH$

(R11) $O_2 + O_3 \rightarrow OH + 2\ O_2$

(R12) $OH + O_3 \rightarrow HO_2 + O_2$

In the latter photostationary state model simulations, all 40 data runs from the FTNH database were independently analyzed to evaluate both R_E/R_C and $P(O_3)$ for known additions of the surrogate species toluene. These additions were made to our base hydrocarbon level 1 and ranged from 0 to 8 ppbv. The results of these simulations are shown in Figure 12 where the values reported for R_E/R_C and $P(O_3)$ for each addition of toluene represent the average values calculated from all 40 FTNH data runs. These results suggest that at mixing ratios of ~2.7 ppbv of toluene that nearly 80% of the bias in the mean value of R_E/R_C is removed. Figure 12 also indicates that at this level of toluene and for an average zenith angle of 35° the estimated hourly production rate of O_3 would be ~0.5 ppbv. The latter hourly rate suggests that the net O_3 enhancement over a 24-hour period would be between 3 and 4 ppbv. (The authors note that an independent calculation using a time-dependent model and a representative FTNH gas mixture with 2.7 ppbv of added toluene gave very similar $P(O_3)$ results, as obtained from the photostationary state runs). By contrast, our original model run using FTNH data and level 1 NMHCs gave a formation rate for O_3 of < 0.2 ppbv per day. Taking into consideration possible further dilution of what might nominally be described as continental outflow into a near-background marine environment, this very modest diurnal O_3 production rate would not appear to be inconsistent with the O_3 levels observed along the northern hemispheric CITE 3 flight track. At this time, therefore, we cannot rule out the elevated hydrocarbon hypothesis as yet another possible explanation for the bias found in the ratio R_E/R_C for the FTNH data set.

A final observation related to the FTNH data set deserving of further comment involves the sampling time period of 1600 to 1650 UT (e.g., 23.4° to 20°N; see run 11-3 in Table 1a). As seen from Figures 7*a* and 7*b*, during this time period the CO mixing ratio dropped to an average value of 68 ppbv. This level is more typical of southern hemispheric or very high altitude air flow, perhaps even stratospheric. The isentropic back trajectories, however, show no evidence of southern hemispheric awing into this latitude [*Shipman et al.*, this issue]. Still another possibility raised by the recent work of *Newell et al.* [1992]

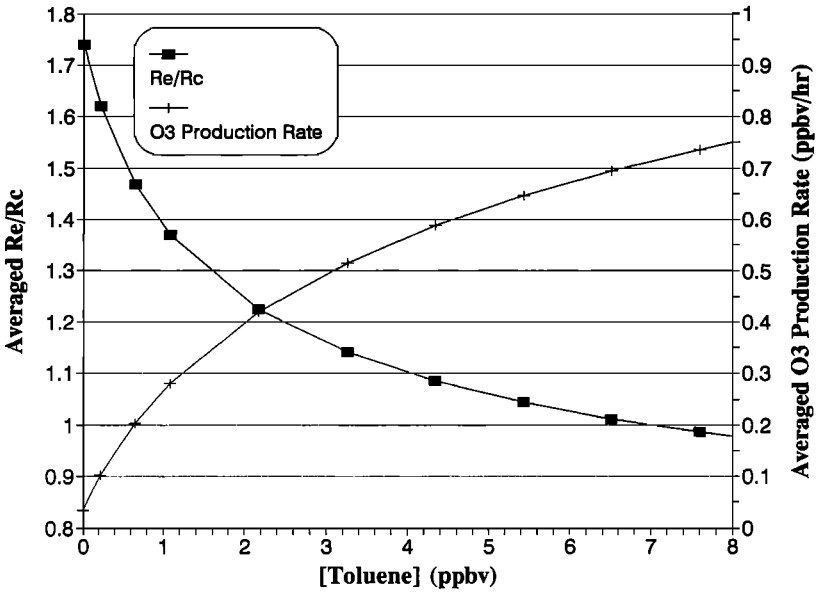

Figure 12. Plot of average R_E/R_C and average O_3 production rate (ppbv/hr).

involves a process that might best be described as "filament transport." Newell et al. suggest that these filaments (i.e., rivers of unique air) may define a very significant transport process for H_2O and possibly other trace constituents within the troposphere.

A very interesting feature of this 20° - 23.4°N sampling interval is the fact that what appears to be relatively clean air resulted in a calculated average value for R_E/R_C of 1.14. Much like the FTSH data, therefore, the observations between 23.4° and 20°N latitude seem to reflect a quite different photochemical environment than that observed for the remainder of the northern hemisphere. Of the 15 data pairs involved in this data subset, eight had S/N NO-NO_2 ratios of 3:1 or greater. Upon removing this small segment of data (e.g., those having S/N ≥3:1) from the overall FTNH data subset resulted in a new mean value for R_E/R_C of 1.80, up from the original value of 1.74.

SUMMARY AND CONCLUSIONS

The CITE 3 NO-NO_2 database has provided a unique opportunity to look at some important aspects of current photochemical theory. Our analysis of these data, as related to evaluating the photochemical ratio R_E/R_C, identified two major data subsets for focused analyses. The regional environmental setting for each data subset has been labeled here as free-tropospheric (2.6-4.9 km) northern hemisphere (FTNH) and free-tropospheric (2.4-5.5 km) southern hemisphere (FTSH). The air mass type for each of these cases was categorized as: middle-altitude middle-latitude continental outflow recently imprinted with ground level sources and lightning (FTNH); and middle-altitude tropical maritime air mixed with a small component of well-aged biomass emissions (FTSH). The results from our analysis of these two higher-quality data sets revealed the following key points: (1) Airborne NO-NO_2 data when used in quantitative assessments of photochemical theory need to be carefully screened in terms of the regional environmental setting in which they are recorded. In some cases the screening of the data in terms of S/N ratios may also be important. (2) The CITE 3 data set, when analyzed as per point 1, produced two reasonably high quality data sets that were found to give quite different results when evaluating the photochemical test ratio R_E/R_C. We have found that the consistency between the observations from the southern hemispheric data subset (i.e., FTSH) and model predictions and the significant inconsistency of the northern hemispheric data subset (i.e., FTNH) points toward a systematic error in the FTNH observational data rather than a shortcoming in our current understanding of fundamental photochemical processes, although the latter possibility cannot be totally ruled out. (3) The FTNH data, which had an R_E/R_C bias of 0.74 ± 0.07, was most likely influenced by (1) An NO_2 interference from a yet unidentified NO_y species; (2) The presence of unidentified/unmeasured hydrocarbons, the integrated chemical reactivity of which would be equivalent to ~2.7 ppbv of toluene; or (3) Some combination of (1) and (2). (4) To reduce the potential impact of problems of the type cited above, future airborne missions should endeavor to (1) make more comprehensive hydrocarbon measurements of C_2-C_{10} species that include both conventional hydrocarbons as well as those containing oxygen and nitrogen; (2) expand field measurements of NO_y to include more of its many component forms (e.g., HNO_3, PAN, NO, NO_2 N_2O_5, HO_2NO_2, RNO_2, $RONO_2$, etc.), thus making the task of examining the question of NO_y-NO_2 interference more tractable; and (3) develop an NO_2 airborne sensor having a much lower susceptibility to interferences from a wide range of NO_y-type compounds. Such a sensor should ideally be designed to operate at outside ambient temperatures, have an extremely short sample residence time, and should allow for the sampling of NO_2 under conditions free of wall effects.

Acknowledgements. This work was supported in part by funds from the National Aeronautics and Space Administration under grants NCC-1-148 and NAG-1438. D.D. Davis would like to thank P. Zimmer and J. Greenberg for their assistance in providing several hydrocarbon sampling flasks for this investigation.

REFERENCES

Blake, D. R., D.F. Hurst, T.W. Smith, Jr., W.J. Whipple, T.Y. Chen, N.J. Blake, and F.S. Rowland, Summertime measurements of selected non-methane hydrocarbons in the Arctic and Subarctic during the 1988 Arctic Boundary Layer Expedition (ABLE 3A), J. Geophys. Res., 97,16,559-16,588, 1992.

Bradshaw, J. D., M. O. Rodgers, S. T. Sandholm, S. KeSheng, and D. D. Davis, A two-photon laser-induced fluorescence field instrument for ground-based and airborne measurements of atmospheric NO, J. Geophys. Res., 90, 12,861-12,873, 1985.

Cadle, R. D., and H. S. Johnston, Chemical reaction in Los Angeles smog, paper presented at the Second Symposium on National Air Pollution, 1952.

Calvert, J. G., Test of the theory of ozone generation in Los Angeles atmosphere, Environ. Sci. Technol., 10, 248-262, 1976.

Calvert, J. G., and S. Madronich, Theoretical study of the initial products of the atmospheric oxidation of hydrocarbons, J. Geophys. Res., 92, 2211-2220, 1987.

Calvert, J. G., and W. R. Stockwell, Deviations from the O_3-NO-NO_2 photostationary state in tropospheric chemistry, Can. J. s Chem., 61, 983-992, 1983.

Chameides, W., D. Davis, M. Rodgers, J. Bradshaw, S. Sandholm, G. Sachse, G. Hill, G. Gregory, and R. Rasmussen, Net ozone photochemical production over the eastern and central North Pacific as inferred from GTE/CITE 1 observations during fall 1983, J. Geophys. Res., 92, 2131-2152, 1987.

Chameides, W., D. Davis, G. Gregory, G. Sachse, and A. Torres, Ozone precursors and ozone photochemistry over eastern North Pacific Ocean during the spring of 1984 based on the NASA GTE/CITE 1 airborne observations, J. Geophys. Res., 94, 9799-9808, 1989.

Chamiedes W., et al., Observed and model-calculated NO_2/NO ratios in tropospheric air sampled during the NASA GTE/CITE 2 field study, J. Geophys. Res., 95, 10,235-10,247, 1990.

Chameides, W. L., et al., Ozone precursor relationships in the ambient atmosphere, J. Geophys. Res., 97, 6037-6055, 1992.

Davis, D.D., J.D. Bradshaw, M.O. Rodgers, S.T. Sandholm, and S. KeSheng, Free tropospheric and boundary layer measurements of NO over the central and eastern North Pacific Ocean,, J. Geophys. Res, 92, 2049-2070, 1987.

Demore, W. B., M. J. Molina, S. P. Sander, D. M. Golden, R. F. Hampson, M. J. Kurylo, C. J. Howard, and A. R. Ravishankara, Chemical kinetics and photochemical data for use in stratospheric modeling in Evaluation 10, JPL Publ., 92-20, Jet Propul. Lab., Pasadena, Calif., 1992.

Dickerson, R. R., D. D. Stedman, W. L. Chameides, P. J. Crutzen, and J. Fishman, Actinometric measurements and theoretical calculations of $J(O_3)$, the rate of photolysis of ozone to $O(^1D)$, Geophys. Res. Lett., 6, 833-837, 1979.

Fehsenfeld, F. C., M. J. Bollinger, S. C. Liu, D. D. Parrish, M. McFarland, M. Trainer, D. Kley, P. C.Murphy, D. L. Albritton, and D. H. Lenschow, A study of ozone in the Colorado mountains, J. Atmos. Chem., 1, 87-105, 1983.

Gregory, G., et al., An intercomparison of airborne nitrogen dioxide instruments, J. Geophys. Res., 95, 10,103-10,128, 1990*a*.

Gregory, G., J. Hoell, Jr., A. Torres, M. A. Carroll, B. R.Ridley, M. Rodgers, J. Bradshaw, S. Sandholm, and D. Davis, An intercomparison of airborne nitric oxide measurements: A second opportunity, J. Geophys. Res., 95, 10,129-10,138, 1990*b*.

Hald, A., Statistical Theory With Engineering Applications, John Wiley, New York, 1962.

Hines, W. W. and D.C. Montgomery, Probability and Statistics: Engineering and Management Science, John Wiley, New York, 1972.

Hoell, J. M., Jr., G. L. Gregory, D. S. McDougal, A. L. Torres, D. D. Davis, J. Bradshaw, M. O. Rodgers, B. A. Ridley, and M. A. Carroll, Airborne intercomparison of nitric oxide measurement techniques, J. Geophys. Res., 92, 1995-2008, 1987.

Hoell, J. M., Jr. et al., Operational overview of the NASA GTE/CITE 3 airborne instrument intercomparisons for sulfur dioxide, hydrogen sulfide, carbonyl sulfide, dimethyl sulfide, and carbon disulfide, J. Geophys. Res., this issue.

Hubler, G., D. Fahey, B. Ridley, G. Gregory, and F. Fehsenfeld, Airborne measurements of total reactive odd nitrogen NO_y during the NASA GTE/CITE 2 project, J. Geophys. Res., 97, 9833-9850, 1992.

Jacob, D., and S. Wofsy, Photochemistry of biogenic emissions over the Amazon forest, J. Geophys. Res., 93, 1477-1486, 1988.

Leighton, P. A., Photochemistry of Air Pollution, Academic, San Diego, Calif., 1961.

Logan, J. A., M. J. Prather, S. C. Wofsy, and M. B. McElroy, Tropospheric chemistry: A global perspective, J. Geophys. Res., 86, 7210-7254, 1981.

Lurmann, F. W., A. C. Lloyd, and R. Atkinson, A chemical mechanism for use in long-range transport/acid deposition computer modeling, J. Geophys. Res., 91, 10,905-10,936, 1986.

Madronich, S., Intercomparison of NO_2 photodissociation and U.V. radiometer measurements, Atmos. Environ., 21, 569-578, 1987.

Madronich, S., and J. G. Calvert, Theoretical study of the tropospheric oxidation of hydrocarbons: Oxidant generation and organic product distribution, paper presented at the China Conference on Tropospheric Chemistry, U.S. Dept. of Energy, and U.S. Envir. Protection Angency, Chin. Soc. of Environ. Sci., Beijing, China, June 1989.

Madronich, S., and J.G. Calvert, Permutation reactions of organic peroxy radicals in the troposphere, J. Geophys. Res., 95, 5697-5715, 1990.

Martinez, J., Impact of natural and anthropogenic hydrocarbons on tropospheric ozone production: Results from automated gas chromatograph, Ph.D. thesis, Ga. Inst. of Technol., Atlanta, 1991.

McFarland, M., D. Kley, and J. W. Drummond, Simultaneous NO, NO_2, and O_3 vertical profile measurements from ground level to 6 km, paper presented at the 4th Biennial Rocky Mountain Regional Meeting, Am. Chem. Soc., Boulder, Colo., June 1978.

Newell, R., N. Newell, Y. Zhu, and C. Scott, Tropospheric rivers? A pilot study, Geophys. Res. Lett., 12, 2401-2404, 1992.

Parrish, D. D., M. Trainer, E. J. Williams, D. W. Fahey, G. Hubler, C. S. Eubank, S. C. Liu, P. C. Murphy, D. L. Albritton, and F. Fehsenfeld, Measurements of the NO-O_3 photostationary state at Niwot Ridge, Colorado, J. Geophys. Res., 91, 5361-5370, 1986.

Ridley, B. A., et al., Ratios of peroxyacetyl nitrate to active nitrogen observed during aircraft flight over the eastern Pacific Ocean and continental United States, J. Geophys. Res., 95, 10,179-10,192, 1990.

Ridley, B. A., Recent measurements of oxidized nitrogen compounds in the troposphere, Atmos. Environ., 25(A), 1905-1926, 1991.

Ridley, B., and E. Robinson, The Mauna Loa Observatory photochemistry experiment, J. Geophys. Res., 97, 10,285-10,290, 1992.

Ridley, B., S. Madronich, R. Chatfield, J. Walega, R. Shetter, M. Carroll, and R. Shetter, Measurements and model simulations of the photostationary state during the Mauna Loa Observatory photochemistry experiment: Implications for radical concentrations and ozone production and loss rates, J. Geophys. Res., 97, 10,375-10,388, 1992.

Ritter, J. A., D. H. Stedman, and T. J. Kelly, Ground-level measurements of nitric oxide, nitrogen dioxide and ozone in rural air, in Nitrogenous Air Pollutants: Chemical and Biological Implications, edited by D. Grosjean, Butterworth, Stoneham, Mass., 1979.

Sandholm, S. T., K. S. Dorris, M. O. Rodgers, D. D. Davis, and J. Bradshaw, An airborne compatible photofragmentation two-photon laser-induced fluorescence instrument for measuring background tropospheric levels of NO, NO_x, and NO_2, J. Geophys. Res., 95 (10), 155-161, 1990.

Sandholm, S. T., et al., Summertime tropospheric observations related to NxOy distributions and partitioning over Alaska: Arctic Boundary Layer Expedition 3A, J. Geophys. Res., 97, 16,481-16,510, 1992.

Sandholm, S. T., et al., Summertime partitioning and budget of NO_y compounds in the troposphere over Alaska and Canada: ABLE 3B, J. Geophys. Res., in press, 1993.

Shetter, R. E., D. H. Stedman, and D. H. West, The $NO/NO_2/O_3$ photostationary state in Claremont, CA., J. Air Pollut. Control Assoc., 33, 212-214, 1983.

Shetter, R. E., D. H. McDaniel, C. A. Cantrell, S. Madronich, and J. G. Calvert, Actinometer and Eppley radiometer measurements of the NO_2 photolysis rate during MLOPEX, J. Geophys. Res., 97, 10,349-10,359, 1992.

Shipham, M. C., A. S. Bachmeier, and B. E. Anderson, CITE 3 meteorological highlights, J. Geophys. Res., this issue.

Singh, H. B., et al., Peroxyacetyl nitrate measurements during CITE 2: Atmospheric distribution and precursor relationships, J. Geophys. Res., 95, 10,163-10,178, 1990.

Singh H. B., et al., Relationship of peroxyacetyl nitrate to active and total odd nitrogen at northern high latitudes: Influence of reservoir species on NO_x and O_3, J. Geophys. Res., 97, 16,523-16,530, 1992.

Singh, H.B., Summertime distribution of PAN and other reactive nitrogen species in the northern high-latitude atmosphere of eastern Canada, J. Geophys. Res., in press, 1993.

Stedman, D. H., and J. O. Jackson, The photostationary state in photochemical smog, Int. J. Chem. Kinet., Symp., 1, 493-501, 1975.

Thompson, A.M., and R. W. Stewart, Effect of chemical kinetics uncertainties on calculated constituents in a tropospheric photochemical model, J. Goephys. Res., 96, 13,089-13,108, 1991.

Trainer, M. E., Y. Hsie, S. A. McKeen, R. Tallamraju, D. D. Parrish, F. C. Fehsenfeld, and S. C. Liu, Impact of natural hydrocarbons in hydroxyl and peroxy radicals at a remote site, J. Geophys. Res., 92, 11,879-11,894, 1987.

B. Anderson, J. Barrick, G. Gregory, M. Shipham, and G. Sachse, NASA Langley Research Center, Hampton, VA 23665.

D. Blake, University of California, Irvine, CA 92717.

J. Bradshaw, W. Chameides, G. Chen, D.D. Davis, M. Rodgers, S. Sandholm, and J. Schendal, School of Earth and Atmospheric Sciences, Georgia Institute of Technology, Atlanta, GA 30332.

J. Collins, Science and Technology Corporation, Hampton, VA 23665.

S. Madronich, National Center for Atmospheric Research, Boulder, CO 80307.

L. Wade, Planning Research Corporation, Hampton, VA 23666.

(Received February 21, 1993;
revised July 14, 1993;
accepted August 21, 1993.)